The Cryosphere, 7, 515–535, 2013
www.the-cryosphere.net/7/515/2013/
doi:10.5194/tc-7-515-2013

The Cryosphere Open Access

Variations in snow and firn chemistry along US ITASE traverses and the effect of surface glazing

D. A. Dixon[1], P. A. Mayewski[1], E. Korotkikh[1], S. B. Sneed[1], M. J. Handley[1], D. S. Introne[1], and T. A. Scambos[2]

[1]Climate Change Institute, School of Earth and Climate Sciences, University of Maine, Orono, ME 04469, USA
[2]National Snow and Ice Data Center, University of Colorado, Boulder, Colorado 80303, USA

Correspondence to: D. A. Dixon (daniel.dixon@maine.edu)

Received: 2 February 2011 – Published in The Cryosphere Discuss.: 16 March 2011
Revised: 16 February 2013 – Accepted: 19 February 2013 – Published: 26 March 2013

Abstract. This study provides a baseline from which changes in the chemistry of the atmosphere over Antarctica can be monitored under expected warming scenarios and continued intensification of industrial activities in the Southern Hemisphere. It is the first study to measure more than 25 chemical constituents in the surface snow and firn across extensive regions of Antarctica. We present major ion, trace element, heavy metal, rare earth element and oxygen isotope data from a series of surface snow samples and shallow firn sections collected along four US ITASE traverses across East and West Antarctica. In each sample we measure dissolved concentrations of Na^+, K^+, Mg^{2+}, Ca^{2+}, Cl^-, NO_3^-, SO_4^{2-}, and MS^- using ion chromatography and total concentrations of Sr, Cd, Cs, Ba, La, Ce, Pr, Pb, Bi, U, As, Al, S, Ca, Ti, V, Cr, Mn, Fe, Co, Na, Mg, Li, and K using inductively coupled plasma sector field mass spectrometry (ICP-SFMS). We also measure $\delta^{18}O$ by isotope ratio mass spectrometry.

Satellite remote sensing measurements of microwave backscatter and grain size are used to assist in the identification of glaze/dune areas across Antarctica and determine if these areas can possibly contain useful chemical climate records. The majority of the non-glaze/dune samples in this study exhibit similar, or lower, concentrations to those from previous studies. Consequently, the results presented here comprise a conservative baseline for Antarctic surface snow chemical concentrations.

The elements Cd, Pb, As and Bi are enriched across Antarctica relative to both ocean and upper crust elemental ratios. Local and global volcanic outgassing may account for the majority of the Bi measured in East and West Antarctica and for a significant fraction of the Cd and As. However, significant concentrations of Cd, Pb, and As remain across much of Antarctica.

1 Introduction

Deep ice cores from the high latitudes of both hemispheres provide us with valuable archives of past climate (Mayewski et al., 1993; Jouzel et al., 1989), but the chemical proxies that they contain must be interpreted in the context of their geographic location. For example, in Antarctica, the individual climate records contained in the Byrd and Taylor Dome deep ice cores do not necessarily reflect past conditions over the entire continent (Masson et al., 2000). There is considerable spatial variability between these deep-ice-core sites. Over-snow traverses, such as those conducted by the International Trans-Antarctic Scientific Expedition (Mayewski et al., 2005), provide us with the opportunity to collect a large number of shallow cores from broad geographic areas. These arrays provide the data needed, at a high enough spatial and temporal resolution, to form a more accurate assessment of the regional chemical and climate differences between deep core sites (Dixon et al., 2011; Kaspari et al., 2004; Bertler et al., 2005). This study presents chemistry data from shallow firn cores/snow pits (hereafter referred to as firn sections), and surface snow samples collected along the US ITASE-2002/2003 Byrd to South Pole traverse (ITASE-02), the US ITASE-2003/2004 South Pole to Taylor Dome traverse (ITASE-03), and the US ITASE-2006/2007 and 2007/2008 Taylor Dome to South Pole traverses (ITASE-06/07). We use these data to determine the spatial variability of chemical deposition over extensive and highly inaccessible areas of the Antarctic continent (Fig. 1).

Since the very earliest trans-Antarctic expeditions, glaze/dune areas have been reported on the East Antarctic plateau (Lister and Pratt, 1959; Black and Budd, 1964), characterized by extremely low accumulation (Picciotto et al., 1970) and extensively recrystallized snow (Giovinetto,

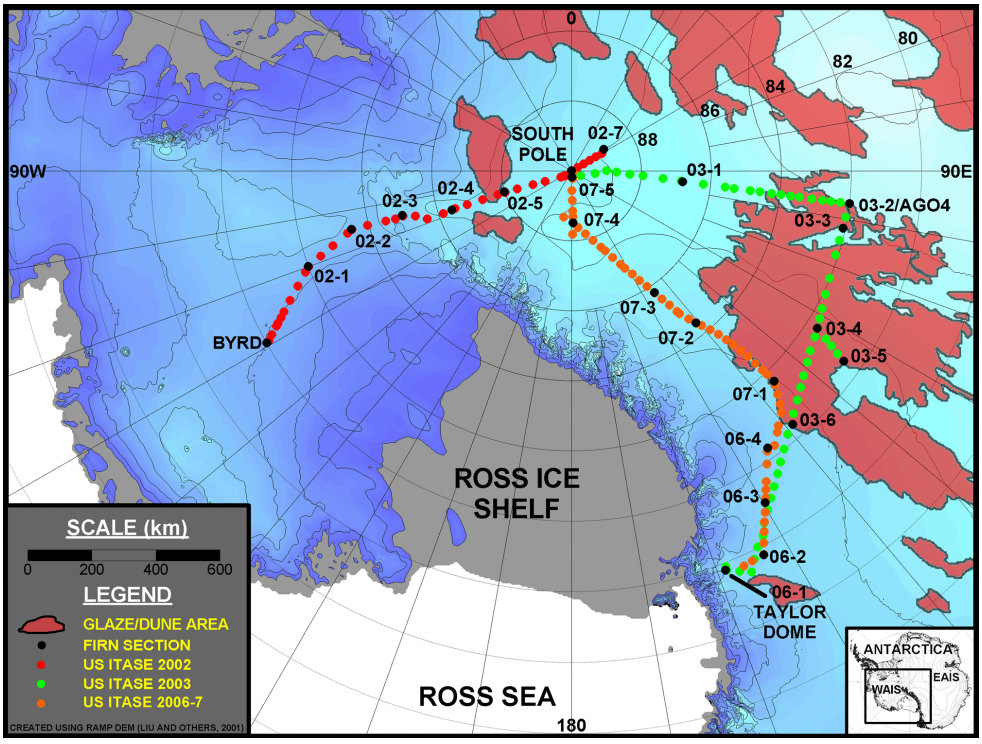

Fig. 1. Polar stereographic map of Antarctica showing the location of surface snow samples and firn sections used in this study. Map also shows the location of known glaze/dune regions. WAIS = West Antarctic Ice Sheet; EAIS = East Antarctic Ice Sheet. Map created using the RAMP digital elevation model (Liu et al., 2001).

1963). However, it was not until the modern satellite remote sensing era that the full extent of these features became apparent. Swithinbank (1988) coined the term "megadunes" for large fields of dune-like features typical of the East Antarctic plateau. These fields cover more than 500 000 km^2 of the Antarctic ice sheet surface (Fahnestock et al., 2000). Megadunes typically have amplitudes of only a few meters, wavelengths of a few kilometers, and parallel crests (which can extend more than 100 km) oriented perpendicular to the regional katabatic wind direction (Frezzotti et al., 2002b). The leeward slope of each megadune consists of a glazed surface representing a long-term accumulation hiatus, while the windward slope is covered with accumulation–redistribution features in the form of severe sastrugi up to 1.5 m high (Frezzotti et al., 2002b). Other glazed (non-megadune) surfaces, representing areas of nil or slightly negative snow accumulation, are also observed across extensive regions of the plateau (Watanabe, 1978; Goodwin, 1990; Frezzotti et al., 2002a). In this study we use an outline map from Bohlander and Scambos (2005) as a first step to determine which of our samples come from known Antarctic glaze/dune regions (Fig. 1). We then use analysis of our chemical profiles to further infer surface conditions along our traverse routes.

1.1 Traverse routes

The ITASE-02 traverse departed Byrd Surface Camp, West Antarctica (80° S, 120° W) on 7 December 2002, and progressed southward (Fig. 1), through the Transantarctic Mountains at the location known as the "Bottleneck", passing South Pole Station on 1 January 2003, ultimately ending up at a location ∼ 100 km beyond the South Pole in the direction of the Pole of Inaccessibility on the East Antarctic plateau (89° S, 60° E) by 4 January 2003.

The ITASE-03 traverse departed the South Pole on 30 November 2003 and proceeded toward the interior of East Antarctica arriving at the Automated Geophysical Observatory number 4 (03-2/AGO4, 82° S, 96.76° E) on 13 December, passing through a glaze/dune area for the last ∼ 400 km of the leg. From 03-2/AGO4, the traverse traveled northward through an extensive glaze/dune area, along the Transantarctic Mountain Seismic Experiment (TAMSEIS) sensor line, passing directly through the Megadunes Camp (80.78° S, 124.49° E), and finishing up at Taylor Dome (77.78° S, 158.73° E) on 20 January 2004.

The first leg of the ITASE-06/07 traverse left Taylor Dome on 13 December 2006 and progressed southward, parallel to and approximately 300 km to the west of the Transantarctic Mountains, finishing in the Byrd Glacier drainage on 7 January 2007. The second leg of the ITASE-06/07 traverse

departed the Byrd Glacier drainage on 17 November 2007 and arrived at the South Pole on 24 December 2007. From 06-4 to 07-3, the 06/07 traverse traveled through the eastern edge of the largest glaze/dune area in East Antarctica.

2 Sampling methodology

Eight firn sections were either drilled or excavated along ITASE-02, six along ITASE-03, and nine along ITASE-06/07 (Table 1). The upper $\sim$1–2.6 m were sampled at each site (because this fragile upper section of the firn is often destroyed during transport), and surface snow samples (upper 2 cm) were collected every $\sim$30–50 km along each traverse route (Fig. 1). All samples are analyzed using an ion chromatograph (IC) for their soluble major ion content (Na^+, K^+, Mg^{2+}, Ca^{2+}, Cl^-, NO_3^-, SO_4^{2-}, $CH_3SO_3^-$ (methylsulfonate: MS^-)). The surface snow samples are additionally analyzed for their stable oxygen isotopes ($\delta^{18}O$) by isotope ratio mass spectrometry (IRMS). All surface snow samples and several shallow firn sections (02-1, 02-5, South Pole, 03-1, 03-3, 06-2, 07-4, and 07-5; Table 1) are also analyzed for a suite of trace elements (Sr, Cd, Cs, Ba, La, Ce, Pr, Pb, Bi, U, As, Al, Ti, V, Cr, Mn, Fe, Co, and Li) by inductively coupled plasma sector field mass spectrometry (ICP-SFMS). The ICP-SFMS also measures the total Na, K, Mg, Ca, and S concentrations in each sample. The accuracy and precision of our IC, IRMS, and ICP-SFMS systems are discussed in more detail by Osterberg et al. (2006).

Lack of accumulation and extensive firn diagenesis at any site exhibiting glazed characteristics likely precludes that site from containing an easily interpreted, annually resolved climate record (Albert et al., 2004; Fahnestock et al., 2000). In addition, the unknown length of hiatus, possibly ranging from decades to centuries (Scambos and Bauer, 2006), represented by each glazed surface presents a problem for a temporally consistent surface snow sampling scheme across the continent. The majority of our surface snow samples and firn sections are collected in positive accumulation areas and therefore represent chemical concentrations typical of summer seasonal precipitation and multi-year averages, respectively (as discussed later). To minimize the possible concentration effects caused by glaze/dune hiatus surfaces, we only collected our surface samples from accumulating snow drifts at all collection sites.

All sample-processing personnel wore non-particulating Tyvek suits, clean plastic gloves, and dust masks. The surface snow samples were collected wearing the same protective gear and always $>$100 m upwind of the traverse vehicles. Samples were only collected if the traverse vehicles could be determined not to have introduced any local contamination. All the ITASE-02 and ITASE-03 surface snow samples for major ion, stable isotope and trace element analysis were collected from the top 2 cm of a loosely consolidated, fresh snowdrift and transferred into two new Whirl-Pak bags using a deionized-ultra-pure-water (DI)-cleaned plastic scoop. The bags were immediately sealed and stored at –20 °C. The ITASE-06/07 surface snow samples for major ion and stable isotope analysis were also collected using this method. However, the ITASE-06/07 surface snow samples for trace element analysis were collected directly into acid-cleaned 60 mL polypropylene Nalgene wide mouth jars and stored at –20° C. No apparent difference in results was detected between the two analytical sampling plans. See supplemental sections S1 and S2 for more information

2.1 Flux vs. concentration

Ideally, we would view these data as chemical flux. However, it would not be accurate to correct these surface snow chemical concentration data for flux, because we do not know when the precipitation occurred or its volume. As a flux correction "experiment", we calculate accumulation rates along the traverse routes using a compilation of net surface mass balance data from Vaughan et al. (1999). We use these accumulation values to apply a flux correction to the surface snow major ion concentration data (Fig. 2). We must note, however, that calculating the flux from a compilation of net surface mass balance data is not the ideal method. However, it is the best we can do with the current dataset. Of all the major ion curves, the flux correction only significantly affects the spatial trend of K in all traverse years, the reason being that, spatially, this ion has extremely low concentration variability. After the flux correction, the resulting K curve looks almost identical to the accumulation curve (Fig. 2). The only other change of note occurs in the ITASE-02 SO_4^{2-} and Cl^- curves, with the rise from 02-3 to 02-7 being subdued. The spatial trends of the remaining ions do not change significantly enough to warrant using the flux correction; i.e., concentrations of sea-salt ions are already higher near the coast in West Antarctica, and concentrations of all ions still remain high in the glaze/dune areas after the correction. So, for the remainder of this paper we will present and discuss chemical concentrations without a flux correction.

2.2 Sample time periods

Several of the firn cores are sub-annually dated based upon seasonal layers in the major ion time series. We approximately date the remaining firn sections using a firn densification depth–age model. We estimate accumulation rates for the model based upon nearby sub-annually dated cores combined with a net surface mass balance model (Vaughan et al., 1999). We use three different time periods from which to calculate the mean, and mean +/–1 standard deviation concentrations in the firn sections: 2000–2006 for all the major ion data, 2000–2006 for the ITASE-06/07 ICP-SFMS data, and 1955–1975 for the ITASE-02 and ITASE-03 ICP-SFMS data. These time periods are chosen to best cover the existing overlap of firn chemistry data from each respective traverse.

Table 1. Information for each ice core used in this study. Accumulation = mean annual accumulation; resolution = sampling resolution; [a] values in brackets correspond to the firn sections used for ICP-SFMS analysis; [b] values in brackets are estimates; [c] no ICP-SFMS K analyses; [d] no ICP-SFMS K or Li analyses; [e] the top 2.1 m of this core were not collected, no IC cation analyses; [f] no K values are reported for the upper portion of this firn section. The 1995–1985 period was used to calculate the K mean value and standard deviation.

Location	Latitude (°N)	Longitude (° E)	Elevation (m)	Depth[a] (m)	Accumulation[b] ($g\,cm^{-2}\,yr^{-1}$)	Age of Section[a] (Years AD)	Time Period Used[a] (Years AD)	Resolution[a] (cm)
ITASE-02								
02-Byrd	–80.009300	–119.424900	1530	0–1	(11)	2003–1998	2003–2000	2.3
02-1[c]	–82.000990	–110.008160	1746	0–1.8 (0.8–12.4)	19	2003–1998 (2001–1966)	2003–2000 (1975–1966)	4 (2.0–4.0)
02-2	–83.500781	–104.986806	1957	0–1.5	(19)	2003–1999	2003–2000	4
02-3	–85.000451	–104.995312	2396	0–1.7	(15)	2003–1999	2003–2000	4
02-4	–86.502500	–107.990313	2586	0–1.8	11	2003–1998	2003–2000	4.1
02-5[d]	–88.002153	–107.983333	2747	0–1.9 (1.1–9.1)	(11)	2003–1996 (1998–1967)	2003–2000 (1975–1967)	4.2 (1.7–2.3)
02-6/South Pole	–89.933250	144.393833	2808	0–2 (0.9–17.7)	(8)	2003–1991 (1997–1911)	2003–2000 (1975–1955)	2 (1.4–1.8)
02-7	–88.998900	59.974400	3000	0–1.7	8	2003–1993	2003–2000	2
ITASE-03								
03-1[d]	–86.840000	95.310000	3124	0–2.5 (2.5–21.2)	5	2004–1983 (1983–1768)	2004–2000 (1975–1955)	2 (1.4–2.9)
03-2/AGO 4	–82.010000	96.760000	3569	0–1.9	(3)	2004–1981	2004–2000	1.3
03-3[e]	–82.080000	101.960000	3444	2.1–15 (2.1–15)	3	1966–1737 (1966–1737)	1966–1955 (1966–1955)	1.5–2.5 (1.5–2.5)
03-4	–81.650000	122.600000	2966	0–1.9	(3)	2004–1981	2004–2000	1.2
03-5[f]	–80.780000	124.490000	2923	0–2.1	(3)	2004–1979	2004–2000	2.0
03-6	–80.390000	138.920000	2393	0–1	(3)	2004–1992	2004–2000	1.6
ITASE-06								
06-1/Taylor Dome	–77.880222	158.458222	2365	0–1.1	(11)	2007–2002	2006–2002	1.6
06-2	–77.781070	152.370500	2277	0–1.2 (0–1.2)	(11)	2007–2002 (2007–2002)	2006–2002 (2006–2002)	1 (1)
06-3	–79.036200	149.680300	2241	0–2.1	(11)	2007–2000	2006–2000	1.2–1.3
06-4	–80.308770	144.691980	2199	0–1.6	(8)	2007–1998	2006–2000	1.4
ITASE-07								
07-1	–81.658000	136.084000	2450	0–1.7	(8)	2008–1998	2006–2000	2
07-2	–84.395070	140.630800	2645	0-1.7	(8)	2008–1998	2006–2000	1.5
07-3	–85.781889	145.719484	2817	0–2.1	(8)	2008–1995	2006–2000	1.8–2.3
07-4	-88.509530	178.530790	3090	0-2.6 (0-1.4)	(8)	2008–1992 (2008–2000)	2006–2000 (2006–2000)	1.2–1.5 (1.2)
07-5	–89.782080	171.431810	2808	0–2.2 (0–1.7)	(8)	2008–1994 (2008–1998)	2006–2000 (2006–2000)	1.2–1.7 (1.2)

Not all firn sections wholly cover the chosen time periods, but all sections cover a minimum of at least three full years of data (see Table 1 for detailed info).

To characterize environmental conditions, we measure a set of physical parameters in addition to the chemistry at each sampling site (Fig. 3). The physical measurements are the following: mean annual accumulation, calculated from the Vaughan et al. (1999) compilation of net surface mass balance; surface elevation, measured in the field by our onboard GPS system (Hamilton and Spikes, 2004); mean annual temperature, calculated from an Antarctic compilation map created using a combination of instrumental mean annual temperatures and 10 m downhole temperatures (Dixon, 2008); RADARSAT-I Antarctic Mapping Project (RAMP) microwave backscatter (Jezek, 1999; Jezek et al., 2002) and Moderate-resolution Imaging Spectroradiometer (Kaufman et al., 1998; Justice et al., 2002) Mosaic of Antarctica (MOA) grain size measurements (Haran et al., 2005; Scambos et al., 2007). The RAMP measurements are extracted from the Antarctic Imaging Campaign-I (AIC-I) dataset. RAMP backscatter values, in decibels, represent the 1997 October mean normalized to an incidence angle of 27° (the center of the beam used most often in the RAMP 1997 AIC-I). The MOA snow grain size data are the mean optical grain size measurements, in microns, from 5 November to 15 December 2003.

3 Results and discussion

3.1 Physical parameters

Examination of each set (ITASE-02, -03, and -06/07) of physical traverse data (as described above) in addition to the $\delta^{18}O$ as measured in the surface snow samples (Fig. 3) reveals a strong similarity between $\delta^{18}O$, accumulation, elevation (inverse) and mean annual temperature, as expected. For ITASE-02, the backscatter curve exhibits significant variability but no strong trend (Fig. 3). For ITASE-03, backscatter and grain size increase towards the interior of East Antarctica and are highest in the glaze/dune area between 03-2 and 03-6 (Fig. 3). The ITASE-06/07 backscatter and grain size are highest between 06-4 and 07-3, which is the part of the traverse that skirts/overlaps a large glaze/dune area (Fig. 3). Although the ITASE-06/07 traverse is only shown to pass through known glaze/dune areas between 06-4 and 07-2 (Fig. 1), we think that this particular route passes through several other glazed, non-dune areas based upon our field observations.

3.2 Seasonality of the samples

As a single summer surface snow sample is likely not representative of the entire summer period, we apply the following

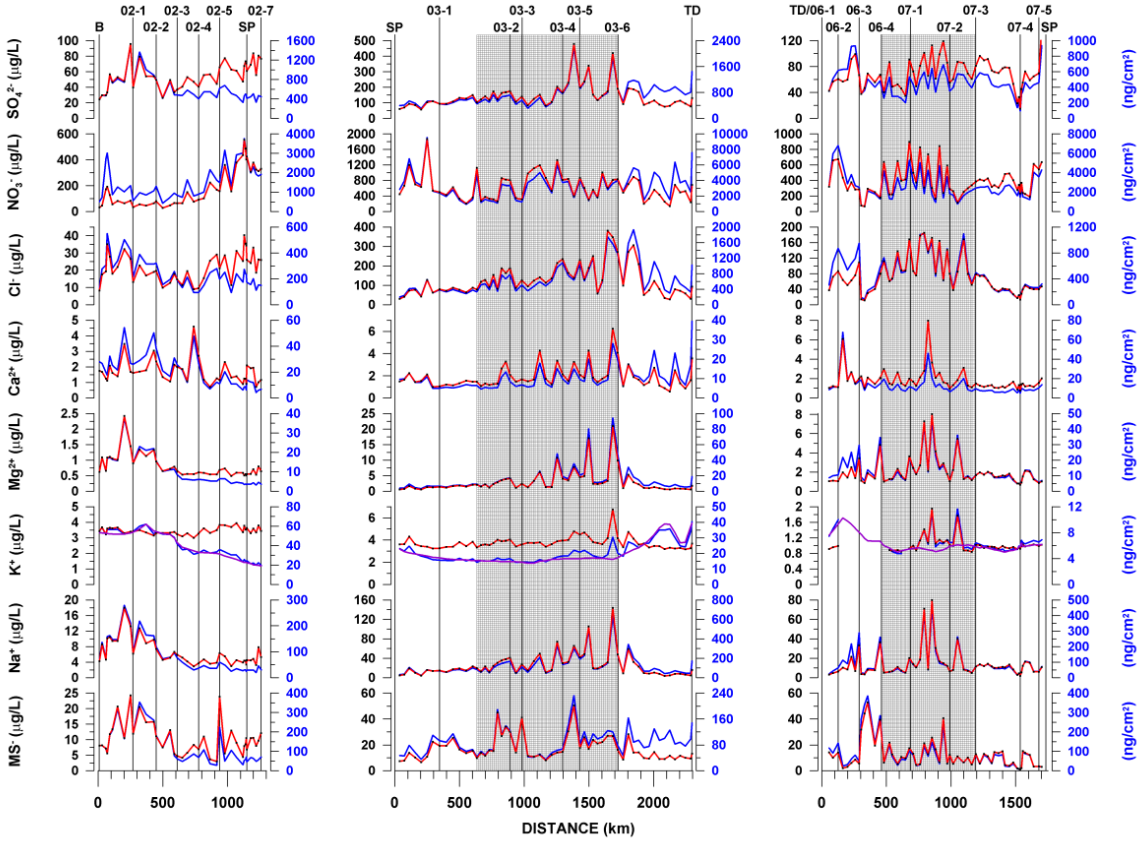

Fig. 2. Surface snow major ion concentration (red) and flux (blue) versus distance for the ITASE-02 (left), ITASE-03 (middle) and ITASE-06/07 (right) traverses. Distances are measured from the beginning of each traverse. Mean annual accumulation (purple) is shown on the K^+ plot for comparison. Vertical lines indicate the locations of firn section collection sites along each traverse: B = Byrd; SP = South Pole; TD = Taylor Dome. Large vertical shaded areas behind plots highlight glaze/dune regions. Note that scales may vary between traverse years.

methodology to assess how representative of typical summer values each surface snow sample is.

High seasonal Na^+ concentrations in Antarctic ice cores are considered to be a deposition timing indicator of the turbulent winter–spring Antarctic atmosphere (Legrand and Mayewski, 1997). Relative to the seasonal variability of Na^+, which is represented in Fig. 4 by the mean +/–1 standard deviation concentrations in the firn sections collected along the traverse routes, the surface snow Na^+ concentrations are low from Byrd to 03-1. Between 03-2 and 03-6 the surface snow Na^+ concentrations range between mean and high, relative to the seasonal variability. This is likely a consequence of sampling in glazed/dune areas. Beyond 03-6, the Na concentrations vary between mean and low values up to Taylor Dome.

Surface snow Na^+ concentrations along the ITASE-06/07 traverse remain low relative to the seasonal variability from Taylor Dome to South Pole apart from three peaks (06-3, 06-4, and one between 07-2 and 07-3) exhibiting mean values and a short section between 07-1 and 07-2 where concentrations are high (Fig. 4). However, all of these higher Na^+ concentrations occur in glazed or glaze/dune areas and are not representative of mean summer concentrations.

Peaks in SO_4^{2-} are observed to occur in the sunlit summer months as photosynthetic organisms prosper in the surface ocean surrounding Antarctica (Legrand and Mayewski, 1997). Relative to the seasonal variability of SO_4^{2-} concentrations in the upper meters of firn, the surface snow SO_4^{2-} concentrations start out slightly below mean at Byrd, quickly increasing to high values, and then fluctuating between mean and high values from 02-1 to South Pole to Taylor Dome (Fig. 4). Several exceptionally high values occur between 03-2 and 03-6, a huge East Antarctic glaze/dune area (Fig. 1). The high concentrations observed in the glaze/dune areas are most likely a result of extremely low or slightly negative accumulation in combination with summer influx of fresh SO_4^{2-} to the hiatus surface. Therefore, the surface samples from glaze/dune areas likely represent multi-year concentrated values.

Along the ITASE-06/07 traverse, surface snow concentrations of SO_4^{2-} are around the mean firn level between Taylor Dome and 06-3. In the glaze/dune areas between 06-3 and 07-3, surface snow concentrations of SO_4^{2-} are low

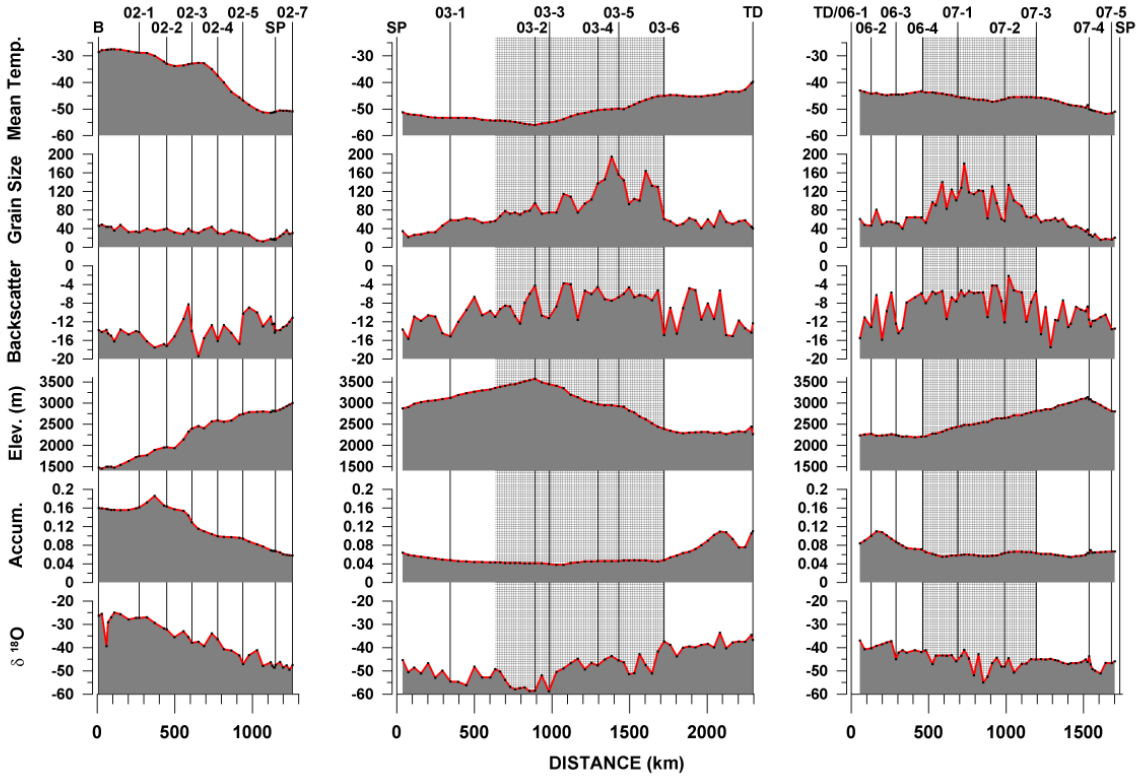

Fig. 3. Surface snow δ^{18}O, mean annual accumulation, surface elevation, RAMP microwave backscatter, MOA grain size and mean annual temperature versus distance for the ITASE-02 (left), ITASE-03 (middle) and ITASE-06/07 (right) traverses. Distances are measured from the beginning of each traverse. Vertical lines indicate the locations of firn section collection sites along each traverse: B = Byrd; SP = South Pole; TD = Taylor Dome. Large vertical shaded areas behind plots highlight glaze/dune regions.

compared to mean firn values. This is in contrast to the ITASE-03 glaze/dune samples, which exhibit unusually high values. ITASE-06/07 surface snow SO_4^{2-} concentrations return to mean/high values between 07-4 and South Pole. The surface snow concentration differences between the ITASE-03 and ITASE-06/07 glaze/dune areas may simply be a result of precipitation differences between the traverse years and/or the fact that during the ITASE-03 traverse we pass directly through the center of an extremely well developed glaze/dune field, and during ITASE-06/07 we skirt the periphery of the aforementioned field.

3.3 Major ions

All the major ions, with the exception of K^+ and Ca^{2+}, exhibit lower summer surface snow concentrations in West Antarctica compared to East Antarctic non-glaze/dune areas (Table 2). Non-glaze/dune surface snow Ca^{2+} concentrations exhibit similar concentrations across Antarctica. All major ion surface snow concentrations from glaze/dune areas are above those from non-glaze/dune areas (Table 2). Several of the ITASE-06/07 firn sections display unusually high concentrations of MS; this is most likely an effect of the extensive, glazed, non-dune surfaces along this traverse route.

3.4 ITASE-02 major ions

The chemistry in Antarctic snow arrives in a variety of forms (e.g., aerosols (dry deposition), precipitation (wet deposition), and gases), and each of these arrives via an atmospheric transport pathway. For example, SO_4^{2-} and Cl^- ions move through the Antarctic atmosphere via the lower troposphere (planetary boundary layer), the upper troposphere (free troposphere), and the stratosphere. They both have multiple sources. Marine biogenic SO_4^{2-} is transported through the lower and upper troposphere, while SO_4^{2-} from volcanic and anthropogenic activity is transported primarily through the stratosphere. Marine Cl^- is emitted into the lower troposphere where it reacts to form HCL and is further transported through the upper troposphere. Cl^- species in the stratosphere also come from volcanic and anthropogenic activity. For ease of discussion, from this point onward we will refer to the three primary atmospheric transport pathways as follows: stratospheric, upper tropospheric, and lower tropospheric.

Examination of the major ions (Na^+, K^+, Mg^{2+}, Ca^{2+}, Cl^-, NO_3^-, SO_4^{2-}, and MS^-) for ITASE-02 (Fig. 4) reveals a decreasing trend for Na^+ and Mg^{2+} from Byrd to 02-7 and the opposite trend for NO_3^-. This trend is to be expected for

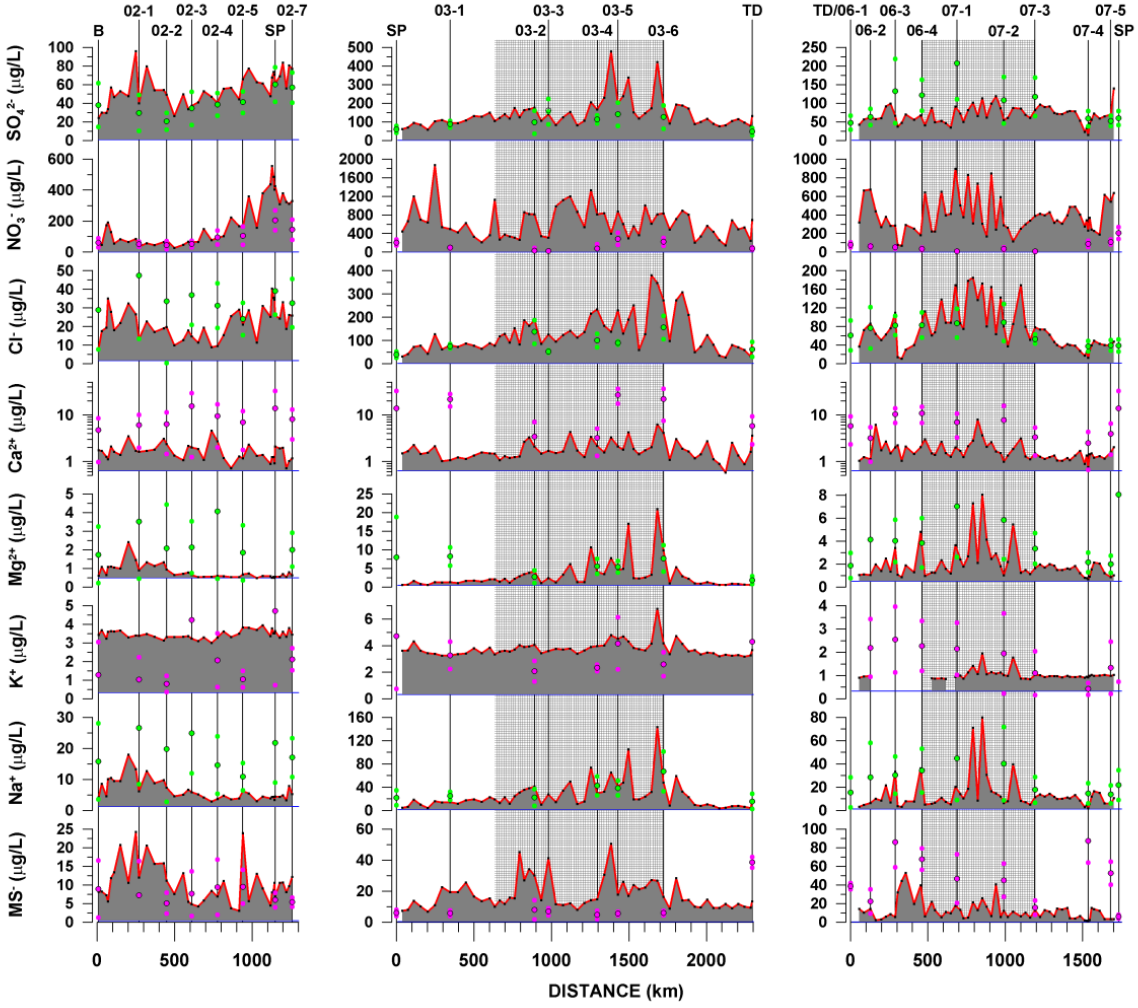

Fig. 4. Surface snow major ion concentration versus distance for the ITASE-02 (left), ITASE-03 (middle) and ITASE-06/07 (right) traverses. Distances are measured from the beginning of each traverse. Vertical lines indicate the locations of firn section collection sites along each traverse: B = Byrd; SP = South Pole; TD = Taylor Dome. The three (pink or green) dots in line with each firn collection site indicate the mean (black outline) and +/–1 standard deviation concentrations in that firn section (if the lower dot is not visible, its value is below zero). Large vertical shaded areas behind plots highlight glaze/dune regions. Horizontal (blue) lines signify detection limits. Note that scales may vary between traverse years.

marine-source ions as elevation and distance from the coast increase. The trend in NO_3^- is also expected due to its stratospheric transport pathway. Previous studies by Kreutz and Mayewski (1999) and Bertler et al. (2005) show a similar relationship between elevation, accumulation, NO_3^-, Na^+, and Mg^{2+}.

A second mode of behavior is evident in the Cl^-, SO_4^{2-} and MS ions (Fig. 4). These ions exhibit high values between Byrd and 02-2, dipping between 02-2 and 02-4, then rising again and remaining high from 02-5 to 02-7 (Fig. 4). SO_4^{2-} and Cl^- display this double-peak pattern most strongly, confirming that their dominant transport pathway is lower tropospheric and that they also have an upper tropospheric transport pathway (Legrand and Mayewski, 1997). It is worth bearing in mind that the chemical concentrations presented here have not been corrected for differences in accumulation. As a result, some fraction of the East Antarctic rise in the ITASE-02 SO_4^{2-} and Cl^- data may be accumulation-related. The double-peak structure of the MS signal is somewhat weak, with the East Antarctic peak dominated by a single high value at 02-5. If we ignore the peak at 02-5, assuming that this single high value may have been caused by an unusually high influx of lower tropospheric air as the sample was collected or by the glaze/dune field in this area, the pattern of ITASE-02 MS concentrations then becomes similar to the marine-source Na^+ and Mg^{2+} ions. K^+ exhibits very little structure and variability from Byrd to 02-7 (Fig. 4), despite the traverse passing close to the Transantarctic Mountains between 02-3 and 02-4 (Fig. 1). Major ion

Table 2. Major ion concentrations for surface snow samples and firn sections.

Surface Snow								
min-max (mean)	Na (ug L^{-1})	K (ug L^{-1})	Mg (ug L^{-1})	Ca (ug L^{-1})	MS (ug L^{-1})	Cl (ug L^{-1})	NO_3 (ug L^{-1})	SO_4 (ug L^{-1})
ITASE-02	2.89–17.9 (6.38)	3.00–3.95 (3.47)	0.49–2.42 (0.80)	0.71–4.60 (1.69)	3.02–24.3 (10.3)	8.25–40.4 (21.9)	27.6–554 (185)	24.3–95.8 (54.7)
ITASE-03 (non-glaze/dune)	3.64–59.2 (13.6)	3.17–4.72 (3.54)	0.56–5.35 (1.36)	0.58–3.58 (1.60)	6.73–28.2 (13.3)	27.5–307 (90.7)	140–1869 (569)	57.6–194 (107)
ITASE-03 (glaze/dune)	10.1–144 (37.3)	3.34–6.77 (3.98)	1.06–21.0 (4.64)	1.07–6.25 (2.24)	8.04–50.5 (21.4)	59.4–381 (164)	262–1330 (685)	81.3–478 (177)
ITASE-06/07 (non-glaze/dune)	1.85–36.3 (10.6)	0.91–1.03 (0.97)	0.68–4.82 (1.60)	0.76–6.09 (1.56)	1.13–52.9 (12.3)	11.1–110 (47.2)	68.4–673 (358)	14.7–140 (65.8)
ITASE-06/07 (glaze/dune)	5.06–79.9 (17.7)	0.84–1.95 (1.07)	0.98–8.04 (2.59)	0.98–7.97 (2.16)	4.43–40.6 (12.5)	37.8–185 (108)	116–896 (428)	34.6–119 (72.8)

Firn sections								
(mean)	Na (ug L^{-1})	K (ug L^{-1})	Mg (ug L^{-1})	Ca (ug L^{-1})	MS (ug L^{-1})	Cl (ug L^{-1})	NO_3 (ug L^{-1})	SO_4 (ug L^{-1})
Byrd (2000–2003)	15.81	1.27	1.73	4.73	8.88	28.97	60.60	37.89
02-1 (2000–2003)	26.62	1.03	3.51	6.03	7.22	47.40	50.39	29.54
02-2 (2000–2003)	19.81	0.80	2.09	6.36	5.10	33.61	45.58	20.64
02-3 (2000–2003)	24.92	4.24	2.14	15.34	7.66	36.95	51.97	34.49
02-4 (2000–2003)	14.62	2.07	4.07	9.42	9.42	31.25	94.11	38.65
02-5 (2000–2003)	10.85	1.06	1.84	6.89	9.51	24.09	105.32	41.13
02-6/SP (2000–2003)	21.78	4.72	8.05	13.84	5.94	39.13	205.04	60.06
02-7 (2000–2003)	17.07	2.12	2.01	8.02	5.37	32.60	144.00	56.83
03-1 (2000–2004)	25.01	3.27	8.26		5.77	74.61	93.08	86.98
03-2/AGO4 (2000–2004)	22.37	2.08	2.79	3.44	7.99	137.08	30.28	97.37
03-3 (1955–1966)					6.88	52.23	19.37	160.97
03-4 (2000–2004)	42.44	2.32	5.59	3.20	4.69	100.03	76.19	112.78
03-5 (2000–2004)	38.59	4.17	5.46		5.64	89.41	286.70	140.26
03-6 (2000–2004)	67.05	2.59	7.71		5.92	156.52	219.63	125.71
06-1/TD (2002–2006)	15.55	4.29	1.88	5.80	38.54	61.17	76.88	47.56
06-2 (2001–2006)	28.41	2.19	4.13	3.18	22.32	77.20	61.10	62.89
06-3 (2000–2006)	30.36	2.55	4.02	10.26	85.96	82.37	49.72	132.43
06-4 (2000–2006)	34.24	2.27	3.85	10.80	67.70	83.07	35.90	121.51
07-1 (2000–2006)	44.73	2.14	7.01	6.93	46.69	87.28	7.95	207.14
07-2 (2000–2006)	40.34	1.95	5.83	7.72	44.91	88.60	36.23	108.14
07-3 (2000–2006)	17.74	1.10	3.36	3.32	15.72	53.16	7.86	117.28
07-4 (2000–2006)	14.69	0.42	2.16	2.50	87.33	37.79	87.05	58.64
07-5 (2000–2006)	13.74	1.34	1.99	3.93	52.54	39.64	108.69	52.20

spatial variability maps in Bertler et al. (2005) exhibit a similar spatial pattern to the aforementioned ITASE-02 major ions. Ca^{2+} concentrations display the greatest variability and the largest peaks in West Antarctica (Fig. 4). This highlights the variable nature of Ca^{2+} deposition and emphasizes the fact that a significant percentage of Ca^{2+} reaches Antarctica via the lower troposphere (Dixon et al., 2011).

3.4.1 ITASE-03 major ions

The major pattern in the ITASE-03 major ion chemistry signal occurs in the majority of the ions. The signal structures of Na^{+}, Mg^{2+}, Cl^{-}, and SO_4^{2-} exhibit a steady rise from South Pole to 03-2; the rate of rise then increases along with the magnitude of the variability from 03-2 to 03-6. A sudden drop around 03-6 leads into a steady decline all the way to Taylor Dome (Fig. 4). The grain size (and to a weaker extent backscatter) displays a similar structure (Fig. 3), suggestive of a strong positive association between concentration and grain size for Na^{+}, Mg^{2+}, Cl^{-}, and SO_4^{2-} in East Antarctica. Empirical orthogonal function analysis confirms this observation, which highlights the effect of glaze/dune areas on chemistry. MS^{-} and Ca^{2+} also follow this pattern, albeit with a couple of subtle differences. The Ca^{2+} curve exhibits two distinct peaks between SP and 03-1, and MS^{-} displays a series of low values between 03-3 and 03-4. The K curve is relatively featureless compared to the other major ions with only the very largest concentration peaks registering. The structure of the NO_3^{-} signal, which exhibits two large peaks close to South Pole followed by increased variability in the glaze/dune areas without a strong concentration trend (Fig. 4), highlights the strong stratospheric NO_3^{-} source resulting in high concentrations all over East Antarctica. It also draws attention to the increased concentrations near the South Pole, which may be a result of anthropogenic activity around South Pole Station.

3.4.2 ITASE-06/07 major ions

Overall, the ITASE-06/07 major ion signal (Fig. 4) is similar to ITASE-03 in that the majority of the ions exhibit their highest concentrations and maximum variability between 06-4 and 07-3. This coincides with the glaze/dune area, so we can conclude that the widespread hiatus surfaces in this area of East Antarctica act to increase concentrations in the majority of the major ions and at the same time slightly increase $\delta^{18}O$ fractionation (Fig. 3).

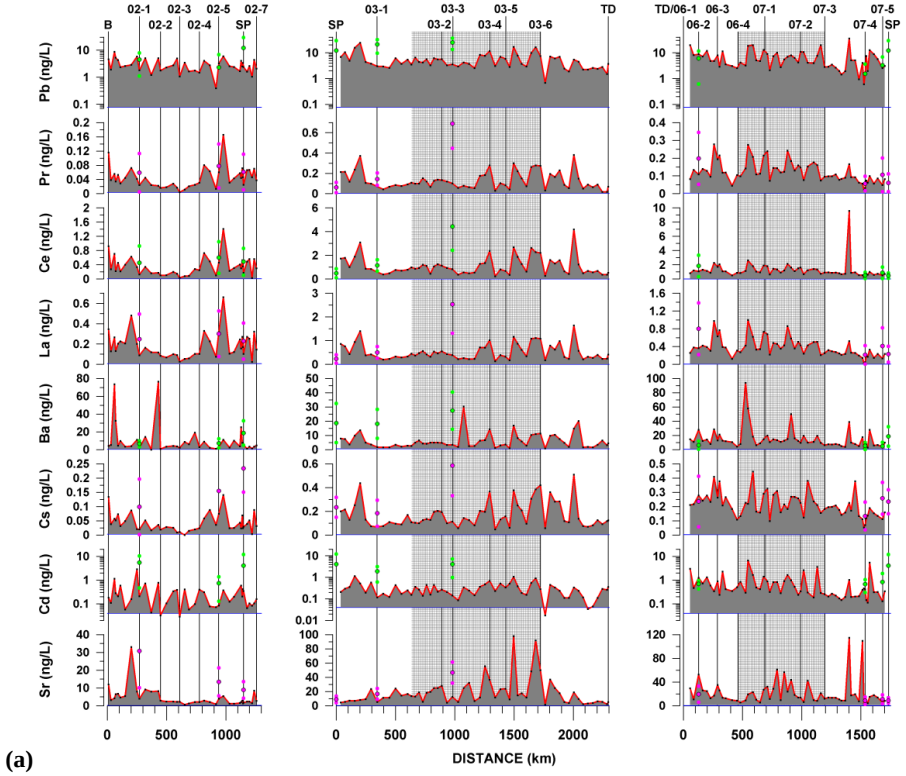

(a)

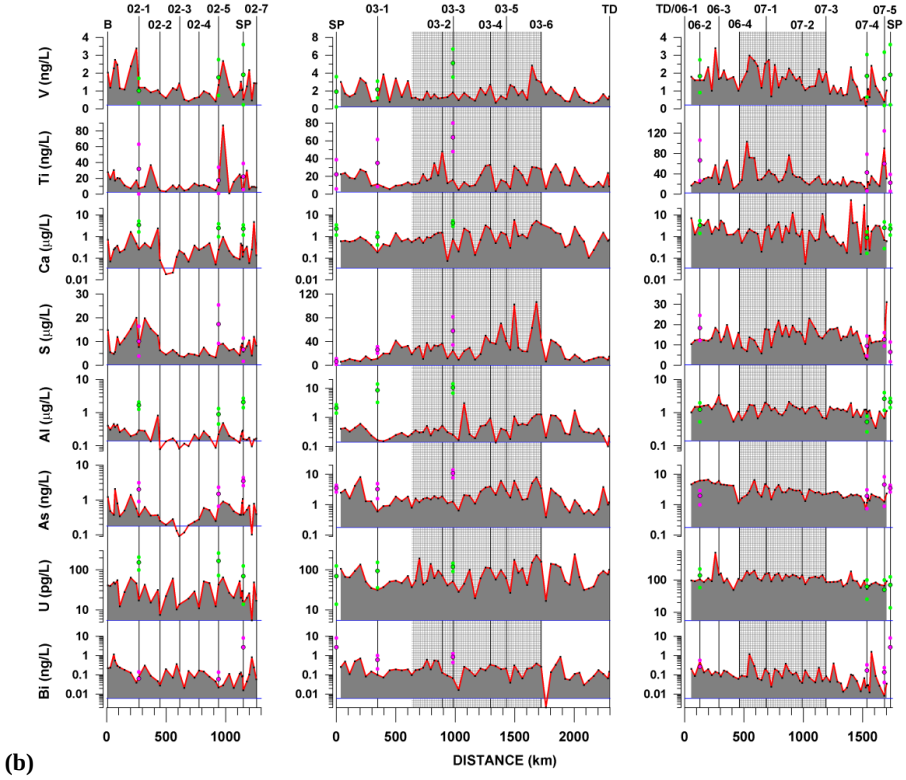

(b)

Fig. 5. Surface snow trace element concentration versus distance for the ITASE-02 (left), ITASE-03 (middle) and ITASE-06/07 (right) traverses. Distances are measured from the beginning of each traverse. Vertical lines indicate the locations of firn section collection sites along each traverse: B = Byrd; SP = South Pole; TD = Taylor Dome. The three (pink or green) dots in line with each firn collection site indicate the mean (black outline) and +/–1 standard deviation concentrations in that firn section (if the lower dot is not visible its value is below zero). Large vertical shaded areas behind plots highlight glaze/dune regions. Horizontal (blue) lines signify detection limits. Note that scales may vary between traverse years.

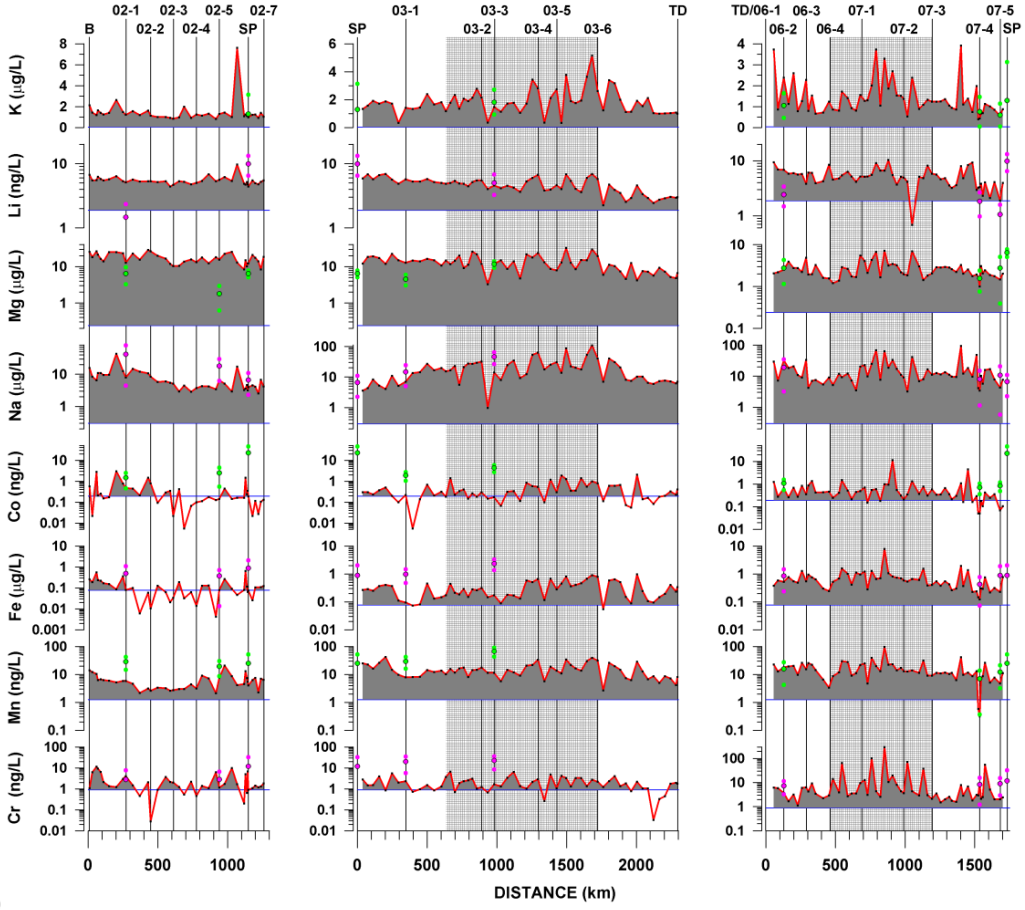

(c)

Fig. 5c. Continued.

3.5 Trace elements

The majority of the mean surface snow trace element concentration data are at, or below, the multi-year mean values calculated from the firn sections (Fig. 5a, b, and c). This suggests that the surface snow concentrations presented here are a conservative estimate of Antarctic values for the majority of the trace elements. Four of the elements (Cs, S, Mg, and K) have no previously published data to compare with (Table 3); this is because S, Mg, and K are typically measured in their soluble forms by IC and are not often measured in their total form by ICP-SFMS analysis. Previous studies of Cs measure only one isotope, ^{137}Cs (Pourchet et al., 1997; Sbrignadello et al., 1994), not total Cs. The measurements of total Cs in this study may be the first analyses of this element conducted over extensive regions of Antarctica.

The mean non-glaze/dune surface snow concentrations for each element for each traverse year reveal that the majority (Sr, Ba, La, Ce, Pr, Pb, As, Li, Al, Ca, Ti, Mn, Fe, Co, and Na) are in the region of, or below, concentrations measured in previous studies (Table 3). Cd, Bi, U, V and Cr exhibit non-glaze/dune concentrations between two and five times higher than previous studies in one or more traverse years (Table 3). The elevated ITASE-06/07 values are likely a consequence of the traverse's route over extensive, glazed, non-dune areas and proximity to the Transantarctic Mountains (Fig. 1). The ITASE-06/07 samples likely contain a greater proportion of dust than the ITASE-02 and ITASE-03 samples as evidenced by higher concentrations of the dust "signature" elements Cs, U, Al, Ca, Ti, and Fe (Table 3). There are likely two factors responsible for the elevated ITASE-03 values in Table 3: the first is the extensive, glazed (low-accumulation/hiatus), non-dune areas occurring throughout the East Antarctic plateau; the second is the large station-associated concentration peak between South Pole and 03-1 that drives up the non-glaze/dune values considerably (Fig. 5a, b, and c). Bi is unusual because it is the only element in our surface snow samples to exhibit elevated values, relative to previous studies, in all traverse years (Table 3). The most likely reason for this is that all of our surface snow samples were collected on the East and West Antarctic plateaus. The previous studies, to which we are comparing our samples, are all coastally located sites. In Antarctica, the primary source of Bi during interglacial

Table 3. Trace element concentrations for surface snow samples, firn sections and from previous studies.

Surface Snow												
min-max (mean)	Sr (ng L^{-1})	Cd (ng L^{-1})	Cs (ng L^{-1})	Ba (ng L^{-1})	La (ng L^{-1})	Ce (ng L^{-1})	Pr (ng L^{-1})	Pb (ng L^{-1})	Bi (ng L^{-1})	U (pg L^{-1})	As (ng L^{-1})	Li (ng L^{-1})
ITASE-02	0.67–33.0 (4.51)	0–2.90 (0.32)	0–0.14 (0.043)	0–76.6 (10.1)	0.024–0.66 (0.18)	0.030–1.41 (0.35)	0.0042–0.17 (0.045)	0.39–8.60 (3.05)	0–1.14 (0.17)	0–65.5 (30.2)	0.092–2.08 (0.54)	4.40–9.75 (5.48)
ITASE-03 (non-glaze/dune)	1.55–37.0 (10.6)	0.017–1.13 (0.27)	0.058–0.51 (0.16)	0.78–20.2 (5.67)	0.18–1.64 (0.51)	0.27–4.19 (1.07)	0.017–0.38 (0.12)	0.69–24.3 (5.24)	0.0021–0.86 (0.20)	16.9–244.8 (75.4)	0.39–8.15 (1.78)	2.26–6.93 (4.38)
ITASE-03 (glaze/dune)	4.22–98.1 (26.0)	0.086–1.05 (0.35)	0.047–0.42 (0.18)	1.00–30.3 (6.56)	0.13–1.16 (0.54)	0.23–2.69 (1.15)	0.028–0.30 (0.14)	2.54–17.0 (6.07)	0.016–0.61 (0.22)	19.5–233 (87.2)	0.64–8.03 (2.55)	3.61–6.90 (4.96)
ITASE-06/07 (non-glaze/dune)	2.21–115 (21.0)	0.11–5.52 (0.71)	0.053–0.41 (0.20)	1.19–39.2 (11.4)	0.031–0.98 (0.31)	0.21–9.58 (1.18)	0.021–0.28 (0.10)	0.60–35.8 (6.24)	0.0082–1.55 (0.14)	48.7–701 (109)	0.71–6.69 (3.08)	1.89–9.37 (5.05)
ITASE-06/07 (glaze/dune)	5.44–60.9 (21.4)	0.19–6.76 (1.12)	0.098–0.45 (0.23)	6.45–94.0 (19.6)	0.21–1.00 (0.47)	0.64–2.60 (1.33)	0.072–0.28 (0.15)	2.09–19.8 (7.94)	0.024–1.17 (0.17)	73.8–197 (129)	1.33–6.54 (2.85)	0.68–10.3 (5.50)
Firn sections												
(mean)	Sr (ng L^{-1})	Cd (ng L^{-1})	Cs (ng L^{-1})	Ba (ng L^{-1})	La (ng L^{-1})	Ce (ng L^{-1})	Pr (ng L^{-1})	Pb (ng L^{-1})	Bi (ng L^{-1})	U (pg L^{-1})	As (ng L^{-1})	Li (ng L^{-1})
02-1 (1966–1975)	30.78	5.50	0.10	6.52	0.25	0.46	0.06	4.50	0.06	153.17	2.01	1.47
02-5 (1967–1975)	13.46	0.75	0.16	7.25	0.30	0.60	0.08	2.27	0.06	168.01	1.49	
02-6/SP (1955–1975)	8.88	4.07	0.23	18.76	0.23	0.49	0.06	12.07	2.71	69.48	3.48	9.86
03-1 (1955–1975)	16.73	1.88	0.18	18.19	0.51	1.15	0.14	20.93	0.59	94.26	3.25	
03-3 (1955–1966) (glaze/dune)	46.61	4.03	0.59	27.44	2.53	4.43	0.69	24.99	0.85	119.01	10.83	5.02
06-2 (2002–2006)	19.59	0.69	0.24	6.36	0.80	1.85	0.20	6.06	0.26	136.75	1.97	2.44
07-4 (2000–2006)	8.46	0.67	0.13	5.34	0.22	0.51	0.06	1.51	0.16	62.40	1.92	1.82
07-5 (2000–2006)	10.93	0.83	0.26	5.12	0.41	0.88	0.11	3.28	0.14	49.64	4.61	1.05
Previous Studies												
(mean)	Sr (ng L^{-1})	Cd (ng L^{-1})	Cs (ng L^{-1})	Ba (ng L^{-1})	La (ng L^{-1})	Ce (ng L^{-1})	Pr (ng L^{-1})	Pb (ng L^{-1})	Bi (ng L^{-1})	U (pg L^{-1})	As (ng L^{-1})	Li (ng L^{-1})
Lambert Basin 1998–2002 (Hur et al., 2007)		0.21		2.40				4.00	0.03	29.00	10.00	
Law Dome 1956–1977 (Vallelonga et al., 2004)	82.68	0.28		2.64				1.84	0.05	26.83		
Coats Land 1958–1975 (Planchon et al., 2002)		0.20		3.13				3.73	0.06	37.14		
Collins Ice Cap, King George Island Jul–Dec 2000 (Hong et al., 2002)		0.10						3.48				
Dolleman Island 1984–1985 (Suttie and Wolff, 1992)		0.08						4.00				
D55 Adelie Land 1940–1980 (Gorlach and Boutron, 1992)		0.30						4.80				
Coats Land 1923–1986 (Wolff et al., 1999)		0.10										
S. Palmer Land Feb 1980 Surface Snow (Wolff and Peel, 1985)		0.26						6.30				
Hercules Neve, Victoria Land 1986–1994 (Van de Velde et al., 2005)				10.87				6.96				
Styx Glacier, Victoria Land 1954–1975 (Van de Velde et al., 2005)				23.27				4.66				
Coats Land 1923–1986 (Wolff and Suttie, 1994)								4.00				
Styx Glacier, Victoria Land 1965–1975 (Barbante et al., 1997)								4.10				
Adelie Land Jan 1983 Surface Snow (Boutron and Patterson, 1987)								5.43				
South Pole Jan 1984 Surface Snow (Boutron and Patterson, 1987)								6.30				
25 cm deep snow pits across Antarctica 1990 (Xiao et al., 2000)								13.68				
Dome-C Holocene Average (Siggaard-Andersen et al., 2007)												7.00
Dome-C Holocene Average (Gabrielli et al., 2010)					0.39	0.91	0.09					

Table 3. Continued.

Surface Snow												
min-max (mean)	Al (µg L^{-1})	S (µg L^{-1})	Ca (µg L^{-1})	Ti (ng L^{-1})	V (ng L^{-1})	Cr (ng L^{-1})	Mn (ng L^{-1})	Fe (µg L^{-1})	Co (ng L^{-1})	Na (µg L^{-1})	Mg (µg L^{-1})	K (µg L^{-1})
ITASE-02	0.079–0.82 (0.23)	3.37–20.0 (8.20)	0.018–4.81 (0.47)	1.11–87.0 (14.8)	0.41–3.37 (1.29)	0.028–11.5 (2.75)	2.15–20.7 (6.21)	0–0.65 (0.13)	0–3.03 (0.41)	2.52–43.4 (7.74)	8.31–28.7 (17.3)	0.82–7.61 (1.44)
ITASE-03 (non-glaze/dune)	0.10–1.73 (0.43)	5.71–42.8 (16.7)	0–2.85 (0.82)	5.75–33.8 (16.0)	0.63–3.85 (1.72)	0.033–5.55 (1.72)	2.67–42.9 (13.9)	0.055–0.98 (0.28)	0.0055–2.06 (0.34)	3.55–40.6 (11.5)	4.19–22.5 (11.1)	0.33–3.40 (1.58)
ITASE-03 (glaze/dune)	0.14–3.14 (0.58)	9.54–106 (35.8)	0.075–5.95 (1.58)	3.68–47.7 (19.5)	0.66–4.85 (1.72)	0.27–6.68 (2.48)	5.70–40.0 (17.5)	0.089–0.93 (0.38)	0.066–1.87 (0.54)	0.97–108 (29.5)	3.27–32.4 (15.1)	0.34–5.15 (2.05)
ITASE-06/07 (non-glaze/dune)	0.35–3.34 (1.29)	2.78–31.1 (13.5)	0.16–48.6 (4.46)	8.38–90.3 (27.9)	0.16–3.40 (1.32)	1.13–55.8 (5.36)	0.32–41.3 (13.3)	0.12–1.94 (0.54)	0.051–4.51 (0.55)	3.42–94.3 (15.9)	1.01–4.92 (2.40)	0.39–3.92 (1.28)
ITASE-06/07 (glaze/dune)	0.60–2.13 (1.27)	5.86–23.0 (14.6)	0.055–13.0 (2.47)	18.7–104 (39.6)	0.69–2.98 (1.83)	2.13–298 (28.9)	4.75–97.3 (20.8)	0.28–8.01 (1.11)	0.15–11.5 (1.01)	3.21–69.8 (18.6)	1.22–7.21 (3.10)	0.52–3.73 (1.55)
Firn sections												
(mean)	Al (µg L^{-1})	S (µg L^{-1})	Ca (µg L^{-1})	Ti (ng L^{-1})	V (ng L^{-1})	Cr (ng L^{-1})	Mn (ng L^{-1})	Fe (µg L^{-1})	Co (ng L^{-1})	Na (µg L^{-1})	Mg (µg L^{-1})	K (µg L^{-1})
02-1 (1966–1975)	1.68	10.17	3.43	31.85	1.01	2.80	28.86	0.49	1.48	41.60	6.42	
02-5 (1967–1975)	0.90	17.32	2.46	17.55	1.75	2.81	19.52	0.37	2.48	18.01	1.80	
02-6/SP (1955–1975)	2.07	6.60	2.29	22.33	1.90	11.87	25.33	0.90	22.55	6.60	6.48	1.29
03-1 (1955–1975)	8.62	25.93	0.95	35.10	2.15	20.16	29.60	0.99	1.89	14.63	4.49	
03-3 (1955–1966) (glaze/dune)	10.52	58.23	4.23	63.94	5.11	22.41	67.26	2.34	4.29	45.43	11.65	1.82
06-2 (2002–2006)	1.25	18.38	3.38	66.31	1.82	7.37	15.95	0.86	1.07	19.03	2.76	1.05
07-4 (2000–2006)	0.53	9.48	0.90	42.83	1.84	8.44	7.09	0.42	0.71	8.05	1.58	0.76
07-5 (2000–2006)	2.61	12.71	2.53	59.73	1.67	9.17	12.41	0.89	0.84	10.72	2.77	0.59
Previous Studies												
(mean)	Al (µg L^{-1})	S (µg L^{-1})	Ca (µg L^{-1})	Ti (ng L^{-1})	V (ng L^{-1})	Cr (ng L^{-1})	Mn (ng L^{-1})	Fe (µg L^{-1})	Co (ng L^{-1})	Na (µg L^{-1})	Mg (µg L^{-1})	K (µg L^{-1})
Lambert Basin 1998–2002 (Hur et al., 2007)	0.17				0.46		3.70	0.05				
Law Dome 1956–1977 (Vallelonga et al., 2004)			2.33		0.65		4.97		0.73	57.33		
Coats Land 1958–1975 (Planchon et al., 2002)	0.52				0.63	1.91	10.37		0.41			
Collins Ice Cap, King George Island Jul–Dec 2000 (Hong et al., 2002)	4.67											
Dolleman Island 1984–1985 (Suttie and Wolff, 1992)	1.00											
D55 Adelie Land 1940–1980 (Gorlach and Boutron, 1992)												
Coats Land 1923–1986 (Wolff et al., 1999)	1.70									60.00		
S. Palmer Land Feb 1980 Surface Snow (Wolff and Peel, 1985)	0.70											
Dome-C Holocene Average (Marino et al., 2004)				120.00				0.75				
WAIS Divide Snow pit 1999–2005 (Koffman et al., 2008)								1.84				

periods is volcanic emissions (Zreda-Gostynska et al., 1997; Hinkley et al., 1999; Vallelonga et al., 2003; Marteel et al., 2008; Gabrielli et al., 2005), which are transported primarily through the upper troposphere and stratosphere. Chemical species transported via the upper atmosphere, such as Bi, should exhibit higher concentrations at high-elevation inland locations, such as the Antarctic Plateau.

The majority of the firn section trace element concentrations (Sr, Ba, La, Ce, Pr, Pb, As, Li, Al, Ca, Ti, Fe, and Na) are comparable to, or below, values from previous studies (Table 3). The 03-3 firn section repeatedly exhibits high

trace element concentrations, relative to other firn sections and values from previous studies. This is expected because it is located in a large glaze/dune area on the East Antarctic plateau (Fig. 1). The remaining firn sections exhibit raised concentrations, relative to previous studies, for several elements (Cd, Bi, U, V, Cr, Mn, and Co). This is likely due to the same reasons, explained above, as the surface snow samples: proximity to the Transantarctic Mountains, location in glazed non-dune areas, station-associated anthropogenic impacts, and/or their interior-plateau positions relative to the coastal locations of most previous studies.

3.5.1 East versus West Antarctic trace element concentrations

To compare East versus West Antarctic trace element input timing differences, we use the mean ITASE-03 non-glaze/dune and ITASE-02 surface snow samples to represent average summer concentrations. We also use the 03-1 (1955–1975) and 02-1 (1966–1975) firn sections to represent the non-glaze/dune multi-year concentrations for East and West Antarctica. Section 02-5 is located on the East Antarctic side of the Transantarctic Mountains (and hence is not representative of West Antarctica). The South Pole firn section is located in close vicinity to a large active station (Amundsen–Scott South Pole Station) with aircraft passing through on a regular basis. Firn section 03-3 represents a well-developed glaze/dune area on the East Antarctic plateau, and sections 06-2, 07-4, and 07-5 cover a more recent time period ($\sim$ 2001–2006) than the ITASE-02 and ITASE-03 firn sections.

Sr and Na, both elements that we know to be primarily marine-source, exhibit higher firn section (multi-year) concentrations in West Antarctica than in East Antarctica (Table 3). The surface snow (summer) concentrations for these two elements are lower overall and exhibit the opposite pattern with higher values in East Antarctica. Therefore, we can conclude that Na and Sr have a dominant lower tropospheric transport pathway and are primarily deposited outside of the summer season. If we apply a similar rationale to the remaining elements, we see that Cd, U, Ca, and Mg exhibit a similar pattern to Sr and Na (Table 3). This is hardly surprising for Ca and Mg, both of which have a significant marine source, but is perhaps a little surprising for Cd and U, both of which have relatively low concentrations in ocean water (Table S2). Despite having slightly higher multi-year East Antarctic concentrations, Cs and Mn are similar to Sr and Na in that the most significant concentration increases occur in West Antarctica outside of the summer season (Table 3).

The rare earth elements La, Ce, and Pr exhibit higher East Antarctic concentrations in both their summer and multi-year samples. These three elements do not show any significant seasonal change in concentration (Table 3). This may suggest an upper tropospheric transport pathway but does not give us any clue as to their input timing. Despite the lack of multi-year data, mean K concentrations are remarkably consistent across East and West Antarctica (including glaze/dune areas) and do not show any significant seasonal change in concentration (Table 3).

Pb, Al, S, and Fe are similar to the rare earths in that they exhibit higher East Antarctic concentrations in both the summer and multi-year samples. However, they are different in that they likely have a strong seasonal input via the upper troposphere outside of the summer season. Cr is also similar to this group of elements, except that it has slightly higher West Antarctic concentrations in summer (Table 3).

As and Ti also exhibit higher East Antarctic concentrations in both the summer and multi-year samples and exhibit a strong seasonal input outside of the summer season. However, the seasonal input does not appear to have a preferred atmospheric transport pathway, displaying increases of a similar magnitude in both East and West Antarctica. Co also behaves as As and Ti, but it displays slightly higher West Antarctic concentrations in summer (Table 3).

The final group of elements (Ba, Bi and V) exhibit summer input via the lower troposphere and a winter input via the upper troposphere, with the latter input being by far the stronger of the two. We know this because the relative summer to multi-year increase is much greater for the East Antarctic sites. Li also follows this pattern, at least for the West Antarctic site. Unfortunately, Li was not included in the 03-1 analyses, so lack of data precludes observation of a multi-year East Antarctic value (Table 3).

3.5.2 ITASE-02 trace elements

The majority of the ITASE-02 "dust" trace elements (Cs, La, Ce, Pr, As, Al, Ti, V, Cr, Mn, Fe and Co) exhibit a double-peak structure. Values are high in West Antarctica (from Byrd to 02-2), dipping between 02-2 and 02-4 and peaking again around 02-4 and 02-5 before leveling off past South Pole and out to 02-7 (Fig. 5a, b, and c). This suggests that multiple transport pathways and/or sources exist for these elements.

The ITASE-02 "marine-source" trace elements (Sr, S, and Na) exhibit a pronounced West Antarctic peak between Byrd and 02-2, while the spatial patterns of Ca and K display only a weak West Antarctic peak. Ca and K have marine and dust sources in Antarctica, which may explain the absence of a strong spatial signature for these two elements. The remaining ITASE-02 trace elements (Cd, Ba, Pb, Bi, U and Li) do not exhibit any significant spatial patterns between Byrd and 02-7.

Several ITASE-02 trace elements (Cs, La, Ce, Pr, Ti, V and Mn) exhibit a large peak in the vicinity of 02-5 (Fig. 5a, b, and c) that is likely caused by the glaze/dune field in this area (Fig. 1). The glaze/dune hiatus areas likely saturate the surface causing higher chemical concentrations in affected samples.

3.5.3 ITASE-03 trace elements

All of the ITASE-03 trace elements exhibit a similar spatial pattern that is characterized by high concentrations across the central East Antarctic glaze/dune area between 03-1 and Taylor Dome (Fig. 5a, b, and c). The majority of the ITASE-03 trace elements (with the exception of Sr, S, Na, Mg and K) also show a distinct peak between South Pole and 03-1. This emphasizes the considerable effect that glaze/dune areas have on chemical concentrations of surface snow in East Antarctica and at the same time draws attention to the magnitude of the concentration increase between South Pole and 03-1 that cannot be attributed to glaze/dune fields and is likely the result of anthropogenic activity associated with South Pole Station.

3.5.4 ITASE-06/07 trace elements

Much like ITASE-03, the spatial pattern of the ITASE-06/07 trace elements is dominated by increased concentrations and variability in the glaze/dune area between 06-4 and 07-2 and distinct peaks around 06-3 and between 07-3 and 07-4 (Fig. 5a, b, and c). This again underscores the fact that glaze/dune areas exercise the dominant control on surface chemistry in these areas of East Antarctica. The ITASE-06/07 concentrations are also complicated by additional factors such as proximity to the Transantarctic Mountains, glazed non-dune areas, and anthropogenic activity in the vicinity of South Pole (Fig. 1).

3.5.5 Glaze/dune and glazed, non-dune areas

The aforementioned traverse profiles (Fig. 3, 4, 5a, b, and c) clearly emphasize the highly variable nature of the glaze/dune areas, not just with respect to the major ion and trace element concentrations, but also with respect to the physical parameters, backscatter and grain size. Examination of the traverse map (Fig. 1) in conjunction with the physical parameter and chemical concentration profiles leads us to classify extensive areas of East Antarctica as "glaze/dune". All samples starting from midway between 03-1 and 03-2 to 03-6 and all samples between 06-4 and 07-3 (shaded areas on traverse profiles) are classified as glaze/dune. The chemistry samples in these glaze/dune areas do not represent typical summer surface snow concentrations, but most likely represent a mean, multi-annual value. Glazed, non-dune areas likely exist between 03-6 and TD, and in the vicinity of 02-5 and 06-3. These areas affect the concentrations of several of our chemical species, but not all. Therefore, we do not definitively classify them as glaze/dune and we do not shade these areas on our spatial plots. The glazed, non-dune data are included in the calculation of our mean "non-glaze/dune" concentrations.

3.5.6 Trace element enrichment factors

To elucidate potential sources for the trace elements in these surface snow samples, we ran enrichment factor (EF) calculations on each set of samples. We calculated the average crustal enrichment factors (EF_c) and average oceanic enrichment factors (EF_o) for each element using mean upper crust elemental abundances (Table S2) from Wedepohl (1995) and mean ocean water elemental abundances from Lide (2005). Values were calculated according to the following: crustal EF for element x [$EF_c(x)$ = mean($[x/r]_{sample}/[x/r]_{upper\ crust}$)], where r = Cs, La, Ce, Pr, V, and Mn to reduce the potential bias from using only a single conservative crustal element; oceanic EF for element x [$EF_o(x)$ = mean($[x/r]_{sample}/[x/r]_{ocean\ water}$)], where r = Sr and Na.

The following elements are enriched in the summer surface snow with respect to earth's upper crust: Cd, Pb, Bi, As, Li, S, Cr, Na, Mg, and K (Table 4). The following are enriched relative to ocean water: Cd, Cs, Ba, La, Ce, Pr, Pb, Bi, U, As, Li, Al, S, Ti, V, Cr, Mn, Fe, Co, and Mg. To separate these two potential sources, we calculated the ocean water fraction of each element according to the following formula: oceanic fraction for element x (x_o = mean(r_{sample} · $[x_{ocean\ water}/r_{ocean\ water}]$), where r = Sr and Na). We then subtracted the oceanic fraction from each element in each sample and recalculated the EF_c to give nss-EF_c values (Table 4). We consider an element highly enriched if it exhibits a nss-EF_c value of 10 or more for each traverse year. We choose a value of 10 following Duce et al. (1975). Elements exhibiting highly enriched nss-EF_c values are Cd, Pb, Bi, As, Li, S, Cr, and Mg, suggesting additional source(s) in addition to the ocean and crust. Of these elements, Cd, Pb, Bi, As, Li, and S are highly enriched for all traverse years. Cr and Mg do not exhibit an nss-EF_c greater than 10 for the ITASE-03 and ITASE-06/07 traverse years, respectively (Table 4). The general pattern of enrichment for several of the highly enriched elements (Cd, Pb, Li and Cr) is such that the ITASE-03 nss-EF_c values are the lowest of the three traverse years. Cr, being the least highly enriched of all the highly enriched elements, does not exhibit nss-EF_c values higher than 10 for ITASE-03. The Mg enrichment values for the ITASE-02 and ITASE-03 surface snow samples are unusually high and for the purposes of this study can be ignored (see supplemental section S2 for more information).

Two recent studies (Planchon et al., 2002; Vallelonga et al., 2004) have published East Antarctic coastal firn EF_c data for Sr, Cd, Ba, Pb, Bi, U, V, Cr, Mn, and Co. All of our surface snow EF_c values fall within the range of these previous studies apart from the ITASE-02 EF_c data for elements Cd, Ba, and Bi, the ITASE-03 glaze/dune EF_c value for Sr, the ITASE-06/07 non-glaze/dune EF_c data for Sr, and the ITASE-06/07 glaze/dune EF_c data for Cr. The ITASE-02 Cd, Ba, and Bi exhibit EF_c values 2 to 5 times higher than previous studies (Table 4). As mentioned above, these

Table 4. Enrichment factors for surface snow samples and previous studies. EF_c = crustal enrichment factor; nss-EF_c = non-sea-salt crustal enrichment factor.

Surface Snow												
EF_c (mean)	Sr	Cd	Cs	Ba	La	Ce	Pr	Pb	Bi	U	As	Li
ITASE-02	2.19	541.64	0.98	2.54	0.76	0.68	1.09	30.82	355.77	1.83	39.17	51.38
ITASE-03 (non-glaze/dune)	1.86	147.75	1.45	0.43	0.79	0.77	0.92	14.80	76.11	1.69	47.68	12.50
ITASE-03 (glaze/dune)	3.58	169.89	1.34	0.46	0.73	0.74	0.94	16.36	95.10	1.69	60.80	12.23
ITASE-06/07 (non-glaze/dune)	4.25	495.88	2.31	1.00	0.56	1.01	1.03	22.10	67.73	3.01	101.78	18.34
ITASE-06/07 (glaze/dune)	2.85	433.46	1.71	1.24	0.59	0.85	0.99	20.60	50.71	2.30	61.05	11.68
Surface Snow												
nss-EF_c (mean)	Sr	Cd	Cs	Ba	La	Ce	Pr	Pb	Bi	U	As	Li
ITASE-02	<0	542.66	0.98	2.54	0.77	0.68	1.09	30.87	356.97	1.70	39.02	50.60
ITASE-03 (non-glaze/dune)	0.10	147.78	1.45	0.42	0.79	0.77	0.92	14.81	76.15	1.60	47.57	11.93
ITASE-03 (glaze/dune)	0.24	169.96	1.34	0.45	0.73	0.75	0.94	16.38	95.19	1.52	60.63	11.15
ITASE-06/07 (non-glaze/dune)	0.91	496.13	2.30	1.00	0.56	1.01	1.03	22.12	67.76	2.84	101.61	17.26
ITASE-06/07 (glaze/dune)	0.51	433.64	1.70	1.24	0.59	0.85	0.99	20.62	50.74	2.18	60.92	10.92
Previous Studies												
EF_c	Sr	Cd	Cs	Ba	La	Ce	Pr	Pb	Bi	U	As	Li
Coats Land 1959–1990 (Planchon et al., 2002)		133.00		0.80				56.00	127.00	4.00		
Law Dome 1898–1989 (Vallelonga et al., 2004)	1.50	269.00						31.00	90.00	2.70		

Table 4. Continued. Enrichment factors for surface snow samples and previous studies. EF_c = crustal enrichment factor; nss-EF_c = non-sea-salt crustal enrichment factor.

Surface Snow												
EF_c (mean)	Al	S	Ca	Ti	V	Cr	Mn	Fe	Co	Na	Mg	K
ITASE-02	0.51	1517.20	2.38	0.79	4.24	14.99	1.83	0.63	5.10	52.88	255.03	9.72
ITASE-03 (non-glaze/dune)	0.28	1096.36	1.54	0.30	2.03	3.03	1.32	0.49	1.44	27.86	52.83	3.45
ITASE-03 (glaze/dune)	0.36	1865.58	2.21	0.28	1.61	4.11	1.52	0.56	2.55	52.28	58.48	3.36
ITASE-06/07 (non-glaze/dune)	1.36	1002.53	9.44	0.68	1.59	13.39	1.42	1.08	2.85	40.86	13.85	3.09
ITASE-06/07 (glaze/dune)	0.71	683.87	3.85	0.55	1.50	34.87	1.61	1.49	3.29	30.95	9.94	2.38
Surface Snow												
nss-EF_c (mean)	Al	S	Ca	Ti	V	Cr	Mn	Fe	Co	Na	Mg	K
ITASE-02	0.51	1418.48	0.89	0.79	4.24	15.01	1.84	0.63	5.11	7.99	245.25	8.25
ITASE-03 (non-glaze/dune)	0.28	1030.31	0.61	0.30	2.02	3.04	1.32	0.49	1.44	<0	46.15	2.47
ITASE-03 (glaze/dune)	0.36	1740.98	0.34	0.28	1.61	4.11	1.53	0.56	2.56	<0	45.77	1.50
ITASE-06/07 (non-glaze/dune)	1.36	876.17	7.60	0.68	1.58	13.39	1.42	1.08	2.85	<0	1.08	1.23
ITASE-06/07 (glaze/dune)	0.71	595.22	2.54	0.55	1.49	34.91	1.61	1.49	3.30	<0	0.98	1.07
Previous Studies												
EF_c	Al	S	Ca	Ti	V	Cr	Mn	Fe	Co	Na	Mg	K
Coats Land 1959–1990 (Planchon et al., 2002)					1.30	16.00	3.00		6.00			
Law Dome 1898–1989 (Vallelonga et al., 2004)					2.30		2.60		18.00			

elevated values may be a result of location differences. The ITASE-02 traverse samples are predominantly located on the West Antarctic plateau, while Law Dome and Coats Land are East Antarctic coastal locations. ITASE-06/07 glaze/dune Cr exhibits an EF_c slightly more than double the value from previous studies. This is probably a combined effect

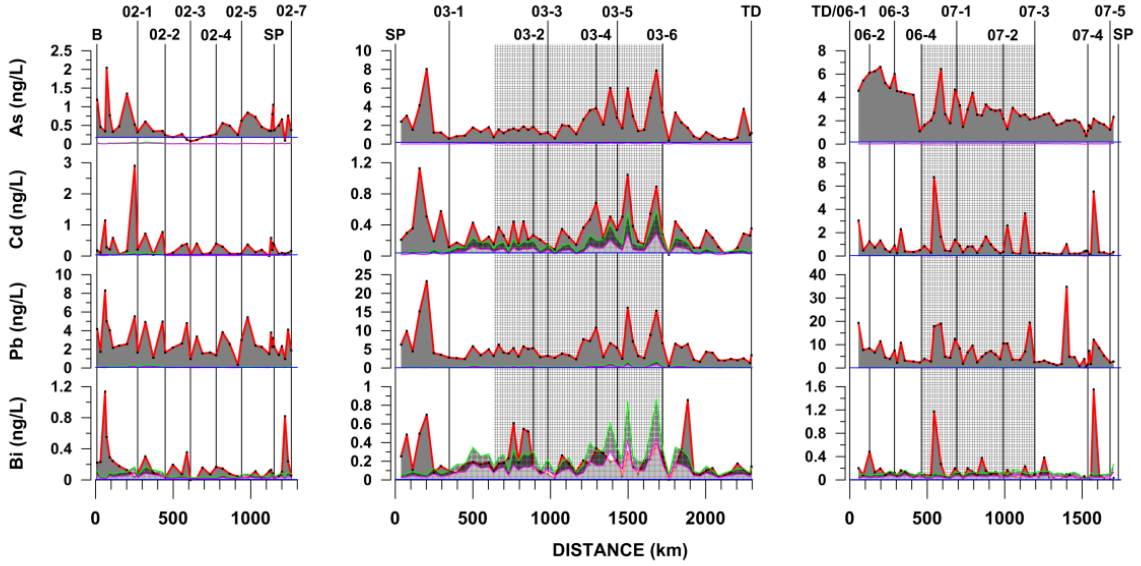

Fig. 6. Surface snow excess element concentration (red) and global mean volcanic quiescent degassing background minimum (pink) and maximum (green) contributions versus distance for the ITASE-02 (left), ITASE-03 (middle) and ITASE-06/07 (right) traverses. Distances are measured from the beginning of each traverse. Vertical lines indicate the locations of firn section collection sites along each traverse: B = Byrd; SP = South Pole; TD = Taylor Dome. Large vertical shaded areas behind plots highlight glaze/dune regions. Horizontal (blue) lines signify detection limits. Note that scales may vary between traverse years.

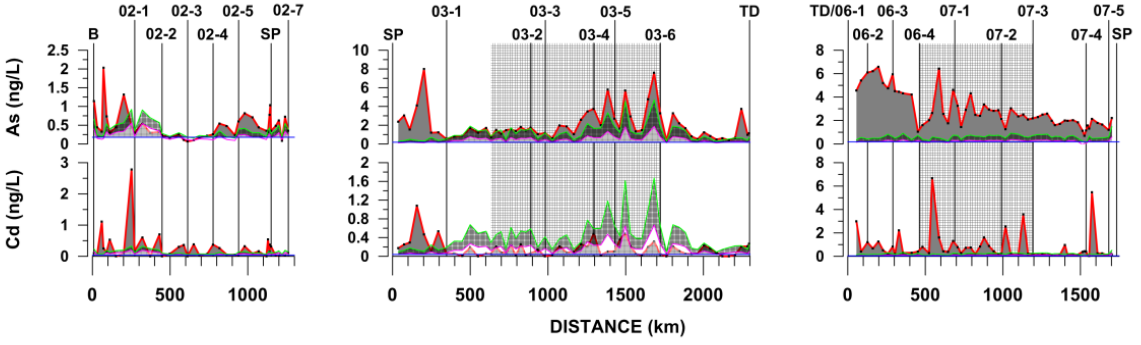

Fig. 7. Surface snow remaining element concentration (red) and Mount Erebus volcanic plume minimum (pink) and maximum (green) contributions versus distance for the ITASE-02 (left), ITASE-03 (middle) and ITASE-06/07 (right) traverses. Distances are measured from the beginning of each traverse. Vertical lines indicate the locations of firn section collection sites along each traverse: B = Byrd; SP = South Pole; TD = Taylor Dome. Large vertical shaded areas behind plots highlight glaze/dune regions. Horizontal (blue) lines signify detection limits. Note that scales may vary between traverse years.

of the glaze/dune hiatus surfaces and their location close to the Transantarctic Mountains. Sr has a significant oceanic source, so we would expect this element to exhibit some enrichment relative to the crust. After the oceanic fraction is removed, Sr does not exhibit significant enrichment. Other elements that exhibit a significantly lower nss-EF_c compared to their EF_c (indicative of an oceanic source) include Ca, Na, Mg, and K, as expected. Several elements display only slightly lower nss-EF_c compared to their EF_c, suggesting a very small oceanic contribution. These include U, Li, and S.

3.5.7 Trace element global volcanic contribution

The elements Cd, Pb, Bi, As, Li, and S are significantly enriched across Antarctica relative to both the oceanic and crustal elemental compositions (Table 4). S in the Antarctic atmosphere is primarily of biogenic origin, but it also has a volcanic source comprising up to 10–15 % (Boutron and Patterson, 1986; Hur et al., 2007). As the majority of our surface snow samples are likely representative of summer precipitation, we use the more conservative values of 5–10 % for our global volcanic background S contributions. Previous studies have measured the ratio of sulfur to trace elements and

heavy metals in volcanic emissions from around the world (Hinkley et al., 1999; Nriagu, 1989). We use the Hinkley et al. (1999) element/S ratios (Table S3) for the highly enriched elements Cd, Pb, Bi, and As to calculate inputs from the global mean volcanic quiescent degassing background. We also use the Mount Erebus plume element/S ratios (Table S3) from Zreda-Gostynska et al. (1997) to represent the local source contributions for Cd and As. Unfortunately, Zreda-Gostynska et al. do not measure Pb or Bi, and neither study measures Li.

Prior to applying the volcanic calculation for each of the following elements, Cd, Pb, Bi, and As, we remove the oceanic fraction (as outlined above) and the crustal fraction, which is calculated according to the following: crustal fraction for element x (x_c = mean(r_{sample}·[$x_{upper\ crust}$/$r_{upper\ crust}$]), where r = Cs, La, Ce, Pr, V, and Mn). We are then left with the excess (excess = total − (oceanic + crustal)) elemental concentrations, from which we calculate the 5 % (minimum) and 10 % (maximum) S values to which we apply the Hinkley et al. element/S ratios (Table S3) to obtain global volcanic background minimum (GVmin) and maximum (GVmax) concentrations.

Comparison between excess element concentrations, GVmin and GVmax (Table 5a) reveals that, for As, the ITASE-02 global volcanic background contribution ranges from 2 % to 4 % of the mean excess As concentration. For ITASE-03 As, the global volcanic background contribution ranges from 1 % to 3 % over non-glaze/dune areas and from 2 % to 4 % over glaze/dune areas. For ITASE-06/07 As, the global volcanic background contribution does not account for more than 1 % over glaze/dune and non-glaze/dune areas (Table 5a). The spatial distribution of the As global volcanic background in our surface snow samples (Fig. 6) reveals that contributions rarely ever become higher than the As detection limit and are therefore not considered a significant source for this element.

Antarctic Cd inputs from the global volcanic background are significant, with GVmax accounting for between 35 % and 57 % of the mean excess Cd concentrations for ITASE-03. However, Cd GVmax is less significant for ITASE-02 and ITASE-06/07, with values of 14 % and 10 %, respectively (Table 5a). Spatially, the distribution of the Cd GVmax input is highest in the glaze/dune areas (Fig. 6). This suggests that a source other than global volcanic background emissions must be responsible for the majority of the Cd in non-glaze/dune areas.

Pb contributions from the global volcanic background reach maximum values of only 5 %, 6 %, and 4 % in the ITASE-02, ITASE-03 and ITASE-06/07 non-glaze/dune areas, respectively (Table 5a). In the ITASE-03 and ITASE-06/07 glaze/dune areas, respective GVmax values reach 11 % and 3 %, which suggests an alternate source is responsible for the majority of the Pb reaching Antarctica.

For ITASE-03, GVmax accounts for 72 % of the Bi input over ITASE-03 non-glaze/dune areas (Table 5a). However, GVmax Bi input is highest in the glaze/dune areas and overestimates several ITASE-03 glaze/dune values significantly (Fig. 6). GVmax Bi input accounts for 76 % and 69 % of the ITASE-06/07 non-glaze/dune and glaze/dune concentrations, respectively (Table 5a). For ITASE-02, GVmax accounts for 40 % of the Bi input. Elsewhere in Antarctica, GVmax input does not account for significant Bi peaks observed in the surface snow samples – specifically, the large double peak between South Pole and 03-1 and the large peak near Byrd (Fig. 6).

3.5.8 Trace element Mount Erebus volcanic contribution

Previous studies have shown that the Mount Erebus (77° 33′ S, 167° 10′ E, 3794 m a.s.l.) plume is enriched in halogens and may therefore be an important source to the Antarctic atmosphere (Kyle et al., 1990; Zreda-Gostynska et al., 1993; Zreda-Gostynska et al., 1997). The Erebus plume also contains a variety of elements such as Na, Al, Cl, K, Ca, Sc, Ti, V, Cr, Mn, Fe, Co, Ni, Cu, Zn, As, Se, Br, Rb, Mo, Cd, In, Sb, Cs, La, Ce, Sm, Eu, Yb, Hf, Ta, W, and Au in varying amounts (Zreda-Gostynska et al., 1997). Of particular interest to this study are the Erebus Cd and As emissions, because these elements exhibit enrichment in all of our samples.

For the sake of the following calculation, we are assuming the Erebus plume is homogeneous over Antarctica, which is likely an oversimplification. We use the Mount Erebus plume element/S ratios (Table S3) from Zreda-Gostynska et al. (1997) to calculate the potential Erebus volcanic contributions of Cd and As to our surface snow samples. We subtract the GVmax Cd and As contributions from our excess Cd and As concentrations to obtain the remaining concentrations for Cd and As (Fig. 7). We calculate the Erebus volcanic contribution for Cd and As using the same method that we used for the global volcanic contribution, except we use 3 % (EVmin) and 5 % (EVmax) S values in the calculation of the Zreda-Gostynska et al. (1997) element/S ratios (Table S3).

Contributions from the Erebus plume potentially account for 75 % and 48 % of the ITASE-02 mean remaining As and Cd values, respectively (Table 5b). Spatial data reveal that significant concentrations of As and Cd remain above the Erebus input – specifically, samples located closer to the coast and near South Pole (Fig. 7).

ITASE-03 EVmax values of As contribute 45 % and 67 % of the mean remaining As concentration for non-glaze/dune and glaze/dune areas, respectively. ITASE-03 EVmax Cd contributions account for >100 % and >300 % of the mean remaining Cd concentrations in non-glaze/dune and glaze/dune areas (Table 5b). Like the ITASE-03 global volcanic background contributions, ITASE-03 Erebus volcanic plume contributions of both As and Cd are highest in the glaze/dune areas but fail to account for the large peaks observed between South Pole and 03-1 (Fig. 7).

Table 5. (a) Excess element concentrations and global mean volcanic quiescent degassing background minimum and maximum contributions. (b) Remaining element concentrations and Mount Erebus volcanic plume minimum and maximum contributions.

5a				
ITASE-02 (mean)	As (ng L^{-1})	Cd (ng L^{-1})	Pb (ng L^{-1})	Bi (ng L^{-1})
Excess Concentration	0.513	0.320	2.879	0.172
Global Volcanic min	0.011	0.023	0.072	0.034
Global Volcanic max	0.023	0.046	0.144	0.068
ITASE-03 (mean)	As (ng L^{-1})	Cd (ng L^{-1})	Pb (ng L^{-1})	Bi (ng L^{-1})
Excess Concentration (non-glaze/dune)	1.725	0.269	4.846	0.195
Global Volcanic min (non-glaze/dune)	0.023	0.047	0.148	0.070
Global Volcanic max (non-glaze/dune)	0.047	0.093	0.296	0.140
Excess Concentration (glaze/dune)	2.488	0.351	5.641	0.219
Global Volcanic min (glaze/dune)	0.050	0.099	0.314	0.149
Global Volcanic max (glaze/dune)	0.099	0.198	0.628	0.298
ITASE-06/07 (mean)	As (ng L^{-1})	Cd (ng L^{-1})	Pb (ng L^{-1})	Bi (ng L^{-1})
Excess Concentration (non-glaze/dune)	3.025	0.706	5.882	0.139
Global Volcanic min (non-glaze/dune)	0.018	0.035	0.111	0.053
Global Volcanic max (non-glaze/dune)	0.035	0.070	0.223	0.106
Excess Concentration (glaze/dune)	2.786	1.121	7.453	0.164
Global Volcanic min (glaze/dune)	0.019	0.038	0.119	0.056
Global Volcanic max (glaze/dune)	0.038	0.075	0.238	0.113

5b		
ITASE-02 (mean)	As (ng L^{-1})	Cd (ng L^{-1})
Remaining Concentration	0.491	0.276
Mean Erebus Volcanic min	0.222	0.079
Mean Erebus Volcanic max	0.370	0.132
ITASE-03 (mean)	As (ng L^{-1})	Cd (ng L^{-1})
Remaining Concentration (non-glaze/dune)	1.678	0.207
Erebus Volcanic min (non-glaze/dune)	0.303	0.108
Erebus Volcanic max (non-glaze/dune)	0.758	0.269
Remaining Concentration (glaze/dune)	2.389	0.158
Erebus Volcanic min (glaze/dune)	0.644	0.229
Erebus Volcanic max (glaze/dune)	1.609	0.572
ITASE-06/07 (mean)	As (ng L^{-1})	Cd (ng L^{-1})
Remaining Concentration (non-glaze/dune)	2.990	0.636
Erebus Volcanic min (non-glaze/dune)	0.227	0.081
Erebus Volcanic max (non-glaze/dune)	0.567	0.202
Remaining Concentration (glaze/dune)	2.748	1.046
Erebus Volcanic min (glaze/dune)	0.244	0.087
Erebus Volcanic max (glaze/dune)	0.611	0.217

The Erebus volcanic plume accounts for no more than 22 % and 32 % of the mean remaining ITASE-06/07 As and Cd concentrations, respectively (Table 5b). This suggests an additional source/sources for the majority of the As and Cd reaching Antarctica.

The volcanic contributions of enriched elements are always greatest in glaze/dune areas. This is most likely a direct effect of S enrichment. The S enrichment in glaze/dune areas is probably a result of the concentrating effect of the hiatus surfaces combined with their proximity to the stratospheric SO_4^{2-} background reservoir. The stratospheric SO_4^{2-} background reservoir is potentially composed of nonexplosive volcanic SO_4^{2-}, an admixture of sources that reside in polar stratospheric clouds (PSC), and continental SO_4^{2-} from sources such as anthropogenic emissions and dust. The volcanic contribution calculation for enriched elements assumes that a fixed percentage of the total S in the atmosphere is of volcanic origin. However, the volcanic contribution calculation frequently overestimates the elemental concentrations in glaze/dune areas. This suggests that either the percentage of volcanic S in the volcanic contribution calculation is set too high and/or significant S input from other sources occurs over timescales comparable in length to the glaze/dune hiatus.

4 Conclusions

This is the first study to measure more than 25 chemical constituents in surface snow and firn across extensive regions of East and West Antarctica and may also be the first to provide total-Cs concentration data. Previous studies involving Cs (Pourchet et al., 1997; Sbrignadello et al., 1994; Faure and Lee, 1999; Pourchet et al., 2003; Woodward, 1964) have focused on only one isotope, ^{137}Cs, either as a measure of fallout from anthropogenic nuclear activities or as a dating tool for ice cores. Researchers usually measure ^{137}Cs fallout in Antarctic soils and sediments to gauge its impact on ecosystems. When using Cs as a dating tool, researchers generally focus on ^{137}Cs concentrations around the time of the 1955 and 1965 bomb-activity peaks. As a result, data regarding total-Cs concentrations in recent Antarctic snow and firn are rare. In this study we find that total Cs may be a useful indicator of dust, based upon its spatial similarity to the traditional "dust" elements such as La, Ce, Pr, V, Mn, etc. (Fig. 5a, b, and c).

Comparisons between surface snow and multi-year firn values of Na^+ (winter–spring input) and SO_4^{2-} (summer input) suggest that a large percentage of these samples represent average summer surface snow concentrations (Fig. 4). The majority of the surface snow trace element concentrations presented here are in the region of, or below, concentrations measured in previous studies and the multi-year means calculated from firn sections (Table 3 and Fig. 5a, b, and c). Therefore, the concentrations presented here are conservative estimates of Antarctic mean summer, mean annual, or glaze/dune values. However, one must bear in mind that samples from glaze/dune areas likely represent multi-year values of unknown age.

Based upon backscatter and grain size values, we have shown that East Antarctic glaze/dune areas tend to increase the magnitude and variability of chemical concentrations in the snow, likely precluding these areas from containing a straightforward interpretation of chemical climate. Backscatter and grain size measurements, good indicators of glaze/dune extent in East Antarctica, may be extremely valuable during the site location phase of Antarctic climate-related ice coring sites.

Glazed, non-dune regions also adversely affect the chemical signature of surface snow and firn, although not as severely as glaze/dune regions. The average grain size in a typical glazed, non-dune region is not as large as that in a well-developed glaze/dune region (Fig. 3). However, as with glaze/dune regions, glazed non-dune regions may be identified by their high (greater than -10) backscatter values (Fig. 3). Although the ITASE-03 and ITASE-06/07 traverses are the only ones shown to pass through extensive glaze/dune areas (Fig. 1), we think that all of our traverse routes pass through some glazed, non-dune areas based upon backscatter values, field observations, and chemical concentration profiles.

In all areas and during all traverse years the δ^{18}O, elevation (inverse) and mean annual temperature are always similar (Table 3). This is a result of Antarctic elevations, and hence temperatures, being strongly associated with distance from the coast and therefore the precipitation source. In West Antarctica (ITASE-02) the grain size and accumulation are strongly related to elevation and temperature, while in central East Antarctica (ITASE-03) only the accumulation retains this strong relationship. Closer to the Transantarctic Mountains (ITASE-06/07), the accumulation is less strongly associated with elevation and temperature and inversely associated with backscatter and grain size. This pattern of accumulation behavior is most likely an outcome of the traverse passing through well-developed glaze/dune areas in addition to glazed, non-dune areas for significant portions of both the ITASE-03 and ITASE-06/07 traverse routes.

Global volcanic outgassing contributions account for a significant fraction of the Bi in both East and West Antarctica and for a significant fraction of the Cd in well-developed East Antarctic glaze/dune areas (Fig. 6). The remaining excess Cd in Antarctic precipitation is likely related to anthropogenic activities, such as mining, in the Southern Hemisphere. Global volcanic outgassing cannot account for the observed concentrations of Pb or As in any area of Antarctica. Previous studies (Wolff and Suttie, 1994) have revealed anthropogenic activity as the primary source of excess Antarctic Pb levels. However, excess Antarctic As concentrations exhibit a pronounced annual signal, particularly in West Antarctica, and are most likely associated with photochemical and/or biogenic activity.

Volcanic outgassing from Mount Erebus does account for a significant fraction of the As and Cd in parts of West and East Antarctica (Fig. 7). Yet, as with the global volcanic outgassing, Erebus plume contributions account for a significantly smaller fraction of these two elements in non-glaze/dune areas (Fig. 7). After accounting for potential volcanic contributions from both global and local sources, concentrations of As remain high near coastal West Antarctica and Taylor Dome (Fig. 7) suggesting either a marine source or a lower tropospheric transport pathway for As.

The As and Cd concentration peaks between South Pole and 03-1 remain unexplained by the combination of crustal, oceanic, global volcanic and local volcanic source contributions (Fig. 7). Additionally, the Bi and Pb concentration peaks between South Pole and 03-1 remain unexplained by the combination of crustal, oceanic and global volcanic source contributions (Fig. 6). One possible explanation for these peaks is increased anthropogenic activity at the South Pole Station during the summer months.

Possible alternate sources for the remaining excess concentration peaks are marine biogenic and/or more distant anthropogenic sources from industrialized regions of the Southern Hemisphere and possibly the Northern Hemisphere. The latter source seems most likely for Cd, Pb and Bi, because a marine biogenic source would cause a pattern more like S, with higher concentrations near the West Antarctic coast, which is not the case.

Additional work to differentiate between non-glaze/dune and glazed, non-dune areas will be valuable. Expanding the scope of this research to achieve full coverage of Antarctica will require the incorporation of external data, such as aerosol monitoring sites, and collaboration with other research groups in similar fields.

Most importantly, our study provides a robust framework for monitoring future changes in the chemistry of the atmosphere over Antarctica. This framework will prove particularly important in the future as we continue to monitor Antarctic atmospheric chemical deposition. Potential changes in atmospheric chemistry are inevitable as Antarctica continues to warm and as Southern Hemisphere industrial activity intensifies.

Supplementary material related to this article is available online at: http://www.the-cryosphere.net/7/515/2013/tc-7-515-2013-supplement..pdf.

Acknowledgements. The International Trans Antarctic Scientific Expedition (ITASE) is funded by NSF OPP (0096299, 0439589, 063740, 063650 and 0837883). We greatly acknowledge the support of the Office of Polar Programs, the 109th Air National Guard (Scotia, New York), M. Wumkes, M. Waszkiewicz of Ice Core Drilling Services (University of Wisconsin), Raytheon Polar Services, and all U.S. ITASE field team personnel.

Edited by: J. Moore

References

Albert, M., Shuman, C., Courville, Z., Bauer, R., Fahnestock, M., and Scambos, T.: Extreme firn metamorphism: impact of decades of vapor transport on near-surface firn at a low-accumulation glazed site on the East Antarctic plateau, edited by: J. Jacka, 39, Ann. Glaciol., 73–78, 2004.

Barbante, C., Turetta, C., Capodaglio, G., and Scarponi, G.: Recent decrease in the lead concentration of Antarctic snow, Int. J. Environ. Anal. Chem., 68, 457–477, 1997.

Bertler, N., Mayewski, P. A., Aristarain, A., Barrett, P., Becagli, S., Bernardo, R., Bo, S., Xiao, C., Curran, M., Qin, D., Dixon, D., Ferron, F., Fischer, H., Frey, M., Frezzotti, M., Fundel, F., Genthon, C., Gragnani, R., Hamilton, G., Handley, M., Hong, S., Isaksson, E., Kang, J., Ren, J., Kamiyama, K., Kanamori, S., Karkas, E., Karlof, L., Kaspari, S., Kreutz, K., Kurbatov, A., Meyerson, E., Ming, Y., Zhang, M., Motoyama, H., Mulvaney, R., Oerter, H., Osterberg, E., Proposito, M., Pyne, A., Ruth, U., Simoes, J., Smith, B., Sneed, S., Teinila, K., Traufetter, F., Udisti, R., Virkkula, A., Watanabe, O., Williamson, B., Winther, J. G., Li, Y., Wolff, E., Li, Z., and Zielinski, A.: Snow chemistry across Antarctica, Ann. Glaciol., 41, 167–179, 2005.

Black, H. P. and Budd, W.: Accumulation in the region of Wilkes, Wilkes Land, Antarctica, J. Glaciol., 5, 3–15, 1964.

Bohlander, J. and Scambos, T.: Outlines of Antarctic megadunes regions, Boulder, Colorado USA: National Snow and Ice Data Center, Unpublished data, 2005.

Boutron, C. F. and Patterson, C. C.: Lead concentration changes in Antarctic ice during the Wisconsin Holocene transition, Nature, 323, 222–225, 1986.

Boutron, C. F. and Patterson, C. C.: Relative levels of natural and anthropogenic lead in recent Antarctic snow, J. Geophys. Res.-Atmos., 92, 8454–8464, 1987.

Dixon, D. A., Mayewski, P. A., Goodwin, I. D., Marshall, G. J., Freeman, R., Maasch, K. A., and Sneed, S. B.: An ice core proxy for northerly air mass incursions into West Antarctica, Int. J. Clim., doi:10.1002/joc.2371, 2011.

Duce, R. A., Hoffman, G. L., and Zoller, W. H.: Atmospheric trace-metals at remote northern and southern-hemisphere sites – pollution or natural?, Science, 187, 59–61, 1975.

Fahnestock, M. A., Scambos, T. A., Shuman, C. A., Arthern, R. J., Winebrenner, D. P., and Kwok, R.: Snow megadune fields on the East Antarctic Plateau: extreme atmosphere-ice interaction, Geophys. Res. Lett. 27, 3719–3722, 2000.

Faure, G. and Lee, G.: Occurrence of cesium-137 and other radionuclides in the surface layers of soil in Ohio and Antarctica, Ohio J. Sci., 99, 111–113, 1999.

Frezzotti, M., Gandolfi, S., La Marca, F., and Urbini, S.: Snow dunes and glazed surfaces in Antarctica: new field and remote-sensing data, edited by: Winther, J. G., and Solberg, R., Ann. Glaciol., 34, 81–88, 2002a.

Frezzotti, M., Gandolfi, S., and Urbini, S.: Snow megadunes in Antarctica: Sedimentary structure and genesis, J. Geophys. Res.-Atmos., 107, 4344, doi:10.1029/2001jd000673, 2002b.

Gabrielli, P., Barbante, C., Boutron, C., Cozzi, G., Gaspari, V., Planchon, F., Ferrari, C., Turetta, C., Hong, S. M., and Cescon, P.: Variations in atmospheric trace elements in Dome C (East Antarctica) ice over the last two climatic cycles, Atmos. Environ., 39, 6420–6429, doi:10.1016/j.atmosenv.2005.07.025, 2005.

Gabrielli, P., Wegner, A., Petit, J. R., Delmonte, B., De Deckker, P., Gaspari, V., Fischer, H., Ruth, U., Kriews, M., Boutron, C., Cescon, P., and Barbante, C.: A major glacial-interglacial change in aeolian dust composition inferred from Rare Earth Elements in Antarctic ice, Quat. Sci. Rev., 29, 265–273, doi:10.1016/j.quascirev.2009.09.002, 2010.

Giovinetto, M. B.: Glaciological studies on the McMurdo-South Pole traverse, 1960–1961, The Ohio State University Research Foundation, Columbus 12, Ohio, 83, 1963.

Goodwin, I. D.: Snow accumulation and surface-topography in the katabatic zone of eastern Wilkes Land, Antarctica, Antarc. Sci., 2, 235–242, 1990.

Gorlach, U. and Boutron, C. F.: Variations in heavy-metals concentrations in Antarctic snows from 1940 to 1980, J. Atmos. Chem., 14, 205–222, 1992.

Hamilton, G. S. and Spikes, V. B.: Evaluating a satellite altimeter-derived digital elevation model of Antarctica using precision kinematic GPS profiling, Glob. Planet. Change, 42, 17–30, 2004.

Hinkley, T. K., Lamothe, P. J., Wilson, S. A., Finnegan, D. L., and Gerlach, T. M.: Metal emissions from Kilauea, and a suggested revision of the estimated worldwide metal output by quiescent degassing of volcanoes, Earth Planet. Sci. Lett., 170, 315–325, 1999.

Hong, S., Lluberas, A., Lee, G., and Park, J. K.: Natural and anthropogenic heavy metal deposition to the snow in King George Island, Antarctic Peninsula, Ocean Polar Res., 24, 279–287, 2002.

Hur, S. D., Cunde, X., Hong, S. M., Barbante, C., Gabrielli, P., Lee, K. Y., Boutron, C. F., and Ming, Y.: Seasonal patterns of heavy metal deposition to the snow on Lambert Glacier basin, East Antarctica, Atmos. Environ., 41, 8567–8578, doi:10.1016/j.atmosenv.2007.07.012, 2007.

Jezek, K. C.: Glaciological properties of the Antarctic ice sheet from RADARSAT-1 synthetic aperture radar imagery, edited by: Jacka, T. H., Ann. Glaciol., 29, 286–290, 1999.

Jouzel, J., Raisbeck, G., Benoist, J. P., Yiou, F., Lorius, C., Raynaud, D., Petit, J. R., Barkov, N. I., Korotkevitch, Y. S., and Kotlyakov, V. M.: A Comparison of deep antarctic ice cores and their implications for climate between 65,000 and 15,000 years ago, Quat. Res., 31, 135–150, 1989.

Justice, C. O., Townshend, J. R. G., Vermote, E. F., Masuoka, E., Wolfe, R. E., Saleous, N., Roy, D. P., and Morisette, J. T.: An overview of MODIS Land data processing and product status, Remote Sens. Environ., 83, 3–15, 2002.

Kaspari, S., Mayewski, P. A., Dixon, D. A., Spikes, V. B., Sneed, S. B., Handley, M. J., and Hamilton, G. S.: Climate variability in West Antarctica derived from annual accumulation-rate records from ITASE firn/ice cores, Ann. Glaciol., 39, 585–594, 2004.

Kaufman, Y. J., Herring, D. D., Ranson, K. J., and Collatz, G. J.: Earth Observing System AM1 mission to Earth, Geoscience and Remote Sensing, IEEE Transactions on, 36, 1045–1055, 1998.

Koffman, B. G., Kreutz, K., Handley, M., Wells, M., Kurbatov, A., and Mayewski, P.: A snowpit record of atmospheric Fe deposition in West Antarctica at the WAIS Divide site, Geochim. Cosmochim. Ac., 72, A487–A487, 2008.

Kreutz, K. J. and Mayewski, P. A.: Spatial variability of Antarctic surface snow glaciochemistry: implications for palaeoatmospheric circulation reconstructions, Antarc. Sci., 11, 105–118, 1999.

Kyle, P. R., Meeker, K., and Finnegan, D.: Emission rates of sulfur-dioxide, trace gases and metals from Mount Erebus, Antarctica, Geophys. Res. Lett., 17, 2125–2128, 1990.

Legrand, M., and Mayewski, P.: Glaciochemistry of polar ice cores: A review, Reviews of Geophysics, 35, 219–243, 1997.

Lide, D. R.: Abundance Of Elements In The Earth's Crust And In The Sea, in: CRC Handbook of Chemistry and Physics, Internet Version 2005, edited by: Lide, D. R., CRC Press, Boca Raton, FL, 2005.

Lister, H. and Pratt, G.: Geophysical Investigations of the Commonwealth Trans-Antarctic Expedition, The Geographical Journal, 125, 343–354, 1959.

Liu, H., Jezek, K., Li, B., and Zhao, Z.: Radarsat Antarctic Mapping Project digital elevation model version 2, Boulder, CO: National Snow and Ice Data Center., Digital media, http://nsidc.org/data/nsidc-0082.html, http://nsidc.org/data/nsidc-0082.html, 2001.

Marino, F., Maggi, V., Delmonte, B., Ghermandi, G., and Petit, J. R.: Elemental composition (Si, Fe, Ti) of atmospheric dust over the last 220 kyr from the EPICA ice core (Dome C, Antarctica), edited by: Jacka, J., Ann. Glaciol., 39, 110–118, 2004.

Marteel, A., Boutron, C. F., Barbante, C., Gabrielli, P., Cozzi, G., Gaspari, V., Cescon, P., Ferrari, C. R., Dommergue, A., Rosman, K., Hong, S. M., and Do Hur, S.: Changes in atmospheric heavy metals and metalloids in Dome C (East Antarctica) ice back to 672.0 kyr BP (Marine Isotopic Stages 16.2), Earth Planet. Sci. Lett., 272, 579–590, doi:10.1016/j.epsl.2008.05.021, 2008.

Masson, V., Vimeux, F., Jouzel, J., Morgan, V., Delmotte, M., Ciais, P., Hammer, C., Johnsen, S., Lipenkov, V. Y., Mosley-Thompson, E., Petit, J. R., Steig, E. J., Stievenard, M., and Vaikmae, R.: Holocene climate variability in Antarctica based on 11 ice-core isotopic records, Quat. Res., 54, 348–358, 2000.

Mayewski, P. A., Meeker, L. D., Morrison, M. C., Twickler, M. S., Whitlow, S. I., Ferland, K. K., Meese, D. A., Legrand, M. R., and Steffensen, J. P.: Greenland ice core signal characteristics - an expanded view of climate-change, J. Geophys. Res.-Atmos., 98, 12839–12847, 1993.

Mayewski, P. A., Frezzotti, M., Bertler, N., Van Ommen, T., Hamilton, G., Jacka, T. H., Welch, B., Frey, M., Qin, D., Ren, J. W., Simoes, J., Fily, M., Oerter, H., Nishio, F., Isaksson, E., Mulvaney, R., Holmund, P., Lipenkov, V., Goodwin, I., and ITASE: The International Trans-Antarctic Scientific Expedition (ITASE): an overview, Ann. Glaciol., 41, 180–185, 2005.

Nriagu, J. O.: A global assessment of natural sources of atmospheric trace-metals, Nature, 338, 47–49, 1989.

Osterberg, E. C., Handley, M. J., Sneed, S. B., Mayewski, P. A., and Kreutz, K. J.: Continuous ice core melter system with discrete sampling for major ion, trace element, and stable isotope analyses, Environ. Sci. Techn., 40, 3355–3361,

doi:10.1021/es052536w, 2006.

Picciotto, E. E., De Breuck, W., and Crozaz, G.: Snow accumulation along the South Pole-Dronning Maud Land Traverse, International Association for Scientific HydroIogy, 86, 18–22, 1970.

Planchon, F. A. M., Boutron, C. F., Barbante, C., Cozzi, G., Gaspari, V., Wolff, E. W., Ferrari, C. P., and Cescon, P.: Changes in heavy metals in Antarctic snow from Coats Land since the mid-19th to the late-20th century, Earth Planet. Sci. Lett., 200, 207–222, 2002.

Pourchet, M., Bartarya, S. K., Maignan, M., Pinglot, J. F., Aristarain, A. J., Furdada, G., Kotlyakov, V. M., Mosley-Thompson, E., Preiss, N., and Young, N. W.: Distribution and fall-out of Cs-137 and other radionuclides over Antarctica, J. Glaciol., 43, 435–445, 1997.

Pourchet, M., Magand, O., Frezzotti, M., Ekaykin, A., and Winther, J. G.: Radionuclides deposition over Antarctica, J. Environ. Radioac., 68, 137–158, doi:10.1016/s0265-931x(03)00055-9, 2003.

Sbrignadello, G., Degetto, S., Battiston, G. A., and Gerbasi, R.: Distribution of 210Pb and 137Cs in Snow and Soil Samples from Antarctica, Int. J. Environ. Anal. Chem., 55, 235–242, 1994.

Scambos, T. A., Haran, T. M., Fahnestock, M. A., Painter, T. H., and Bohlander, J.: MODIS-based Mosaic of Antarctica (MOA) data sets: Continent-wide surface morphology and snow grain size, Remote Sens. Environ., 111, 242–257, doi:10.1016/j.rse.2006.12.020, 2007.

Siggaard-Andersen, M. L., Gabrielli, P., Steffensen, J. P., Stromfeldt, T., Barbante, C., Boutron, C., Fischer, H., and Miller, H.: Soluble and insoluble lithium dust in the EPICA DomeC ice core – Implications for changes of the East Antarctic dust provenance during the recent glacial-interglacial transition, Earth Planet. Sci. Lett., 258, 32–43, doi:10.1016/j.epsl.2007.03.013, 2007.

Suttie, E. D. and Wolff, E. W.: Seasonal input of heavy-metals to Antarctic snow, Tellus B, 44, 351–357, 1992.

Swithinbank, C.: Antarctica, in: Satellite image atlas of glaciers of the world, edited by: Williams Jr, R. S., and Ferrigno, J. G., U.S. Government Printing Office, 1–139, Washington, DC, 1988.

Vallelonga, P., Candelone, J. P., Van de Velde, K., Curran, M. A. J., Morgan, V. I., and Rosman, K. J. R.: Lead, Ba and Bi in Antarctic Law Dome ice corresponding to the 1815 AD Tambora eruption: an assessment of emission sources using Pb isotopes, Earth Planet. Sci. Lett., 211, 329–341, doi:10.1016/s0012-821x(03)00208-5, 2003.

Vallelonga, P., Barbante, C., Cozzi, G., Gaspari, V., Candelone, J. P., Van de Velde, K., Morgan, V. I., Rosman, K. J. R., Boutron, C. F., and Cescon, P.: Elemental indicators of natural and anthropogenic aerosol inputs to Law Dome, Antarctica, Ann. Glaciol., 39, 169–174, 2004.

Van de Velde, K., Vallelonga, P., Candelone, J. P., Rosman, K. J. R., Gaspari, V., Cozzi, G., Barbante, C., Udisti, R., Cescon, P., and Boutron, C. F.: Pb isotope record over one century in snow from Victoria Land, Antarctica, Earth Planet. Sci. Lett., 232, 95–108, doi:10.1016/j.epsl.2005.01.007, 2005.

Vaughan, D. G., Bamber, J. L., Giovinetto, M., Russell, J., and Cooper, A. P. R.: Reassessment of net surface mass balance in Antarctica, J. Climate, 12, 933–946, 1999.

Watanabe, O.: Distribution of surface features of snow cover in Mizuho Plateau, Memoirs of National Institute of Polar Research, Special Issue, 44–62, 1978.

Wedepohl, K. H.: The composition of the continental crust, Geochim. Cosmochim. Ac., 59, 1217–1232, 1995.

Wolff, E. W. and Peel, D. A.: Closer to a true value for heavy metal concentrations in recent Antarctic snow by improved contamination control, Ann. Glaciol., 7, 61–69, 1985.

Wolff, E. W., and Suttie, E. D.: Antarctic snow record of southern-hemisphere lead pollution, Geophys. Res. Lett., 21, 781–784, 1994.

Wolff, E. W., Suttie, E. D., and Peel, D. A.: Antarctic snow record of cadmium, copper, and zinc content during the twentieth century, Atmos. Environ., 33, 1535–1541, 1999.

Woodward, R. N.: Strontium-90 and Caesium-137 in Antarctic Snows, Nature, 204, 1291–1291, 1964.

Xiao, C. D., Qin, D. H., Yao, T. D., Ren, J. W., and Li, Y. F.: Global pollution shown by lead and cadmium contents in precipitation of polar regions and Qinghai-Tibetan Plateau, Chin. Sci. Bull., 45, 847–853, 2000.

Zreda-Gostynska, G., Kyle, P. R., and Finnegan, D. L.: Chlorine, fluorine, and sulfur emissions from Mount Erebus, Antarctica and estimated contributions to the Antarctic atmosphere, Geophys. Res. Lett., 20, 1959–1962, 1993.

Zreda-Gostynska, G., Kyle, P. R., Finnegan, D., and Prestbo, K. M.: Volcanic gas emissions from Mount Erebus and their impact on the Antarctic environment, J. Geophys. Res.-Sol., 102, 15039–15055, 1997.